General Disclaimer

One or more of the Following Statements may affect this Document

- This document has been reproduced from the best copy furnished by the organizational source. It is being released in the interest of making available as much information as possible.

- This document may contain data, which exceeds the sheet parameters. It was furnished in this condition by the organizational source and is the best copy available.

- This document may contain tone-on-tone or color graphs, charts and/or pictures, which have been reproduced in black and white.

- This document is paginated as submitted by the original source.

- Portions of this document are not fully legible due to the historical nature of some of the material. However, it is the best reproduction available from the original submission.

NASA CR 134813

IMPROVING THE TOUGHNESS OF REFRACTORY COMPOUNDS

by T. Vasilos and R.M. Cannon, Jr.

November 3, 1975

AVSD-0108-76-RR

AVCO SYSTEMS DIVISION

prepared for

NATIONAL AERONAUTICS AND SPACE ADMINISTRATION

NASA Lewis Research Center

Contract NAS3-17768

FINAL REPORT

1. Report No.	2. Government Accession No.	3. Recipient's Catalog No.
NASA CR-134813		

4. Title and Subtitle	5. Report Date
IMPROVING THE TOUGHNESS OF REFRACTORY COMPOUNDS	November 1975
	6. Performing Organization Code

7. Author(s)	8. Performing Organization Report No.
T. Vasilos and R.M. Cannon, Jr.	AVSD-0108-76-RR
	10. Work Unit No.

9. Performing Organization Name and Address	11. Contract or Grant No.
AVCO CORPORATION Systems Division Lowell, Massachusetts 01851	NAS3-17768
	13. Type of Report and Period Covered
	Contractor Report

12. Sponsoring Agency Name and Address	14. Sponsoring Agency Code
National Aeronautics and Space Administration Washington, D.C. 20546	

15. Supplementary Notes

16. Abstract

Composition and processing studies were conducted on silicon nitride and silicon carbide materials. Charpy mode impact testing to 2415°F established the effectiveness of higher purity silicon nitride powder sources in reducing the scatter of measurements and in improving short time bend strengths as well as bend stress rupture properties. Stabilized zirconia additions in particular were observed to dramatically enhance low and high temperature bend strengths and stress rupture properties for all grades of siolcon nitride powder.

Silicon carbide samples showed relatively poor impact resistance, although the maxima in stress rupture behavior was exhibited by this material.

17. Key Words (Suggested by Author(s))		18. Distribution Statement
Turbine materials	Stress Rupture	Unclassified - Unlimited
Ceramics	Bend Strength	
Silicon Nitride		
Silicon Carbide		
Impact Resistance		

19. Security Classif. (of this report)	20. Security Classif. (of this page)	21. No. of Pages	22. Price*
Unclassified	Unclassified	51	3.00

*For sale by the National Technical Information Service, Springfield, Virginia 22151

FOREWORD

The research described herein was conducted by the Avco Corporation, Systems Division, under NASA Contract NAS3-17768. The work was performed under the management of the NASA Project Manager, Mr. William A. Sanders, Materials & Structures Division, NASA/Lewis Research Center. Dr. Thomas Vasilos was the Project Leader, with Dr. William Rhodes and Dr. Rowland M. Cannon, Jr. assisting in materials evaluation. Other Avco personnel who contributed significantly to this project were Ernest Vallante, John Centorino, Burton MacAllister and George Ross.

TABLE OF CONTENTS

LIST OF FIGURES

LIST OF FIGURES concl'd

LIST OF TABLES

SUMMARY

The objective of this program was mainly to improve the toughness of silicon nitride and silicon carbide materials through compositional and processing controls. The purpose was to enhance the prospect of these materials being successfully used as turbine stator vanes and blades in advanced turbine engines.

Primary emphasis was given toward improving the mechanical impact resistance at a range of temperatures.

The influence of material microstructure and process variables on bend strength and stress rupture life were also studied.

Material development was conducted with the goal of retaining demonstrated thermal shock stability of the primary phase materials.

Special higher purity grades of silicon nitride powder were employed with significant reductions in cation impurities. Comparisons were established with samples prepared of standard controlled phase grade silicon nitride. A special higher purity fine particle grade of SiC was employed, but at the mid-point of the program, further supply became unavailable.

Impact strength tests demonstrated the effectiveness of the higher purity powder sources in reducing the scatter of measurements, although the target result of 0.7 joules (6 in-lbs) for a 0.135 cm (.25") x 0.135 cm (.25") cross-section was realized in only isolated tests.

Higher purity chemistry of source materials was also found to improve short time bend strengths as well as bend stress rupture properties of silicon nitride. No particular difficulties were encountered in densifying these powders with the particular additives employed.

Stabilized zirconia additions in particular were observed to dramatically enhance low and high temperature bend strengths and stress rupture properties for all grades of Si_3N_4 powder.

SiC samples showed relatively poor impact resistance, although the maxima in stress rupture behavior was exhibited by this material.

INTRODUCTION

The objective of this program was primarily concerned with improving the thoughness of refractory ceramics in terms of impact resistance. Emphasis was placed on silicon nitride, although silicon carbide was also studied.

The approach was to raise the impact strength of fabricated samples through control of chemistry and physical microstructure. Such control was sought through improved powder characteristics, additive composition, and processing parameters. The improvements were to be made in such a way that no serious decomposition, change in structure, loss of thermal shock resistance, loss of creep strength, or of other properties would occur.

FABRICATION

Silicon Nitride

Powder - Advanced Materials Engineering Ltd. was placed under subcontract to produce high α Si_3N_4 powder with the goals of (1) a reduction of calcium impurity by a factor of ten, compared to their standard controlled phase grade; (2) total calcium, sodium and potassium concentration of 0.04 percent or less; (3) freedom from discreet particulate second phases excluding silicon oxynitride and iron silicides; (4) reduction in iron and iron silicide concentration; and (5) alternate crystallite and agglomerate morphology.

Two major lots of powder were prepared from two silicon powder sources and each major lot represented one nitridization firing. Within each major lot were three (3) sublots. Each sublot was considered a batch and represented some powder or powder processing variable. Seven kilograms (15 pounds) of each batch (lot) was received and comparisons were made with a lot of standard controlled phase grade. There were no significant morphological differences observed between the powder lots. Each was composed of highly agglomerated particles.

The salient chemical and physical properties are listed below in Tables 1 and 2. The initial elements listed (Fe, Ca, Mg, Al, Ti, Mn, Na, and K) are the results of a quantitative analysis for the most critical elements. Three lots were surveyed on a semi-quantitative basis for other possible impurities. Overall, significant progress was made in improving the level of impurities over the standard controlled phase grade. Lots AME 9-1, 9-4, 9-5, and 9-6 met the total Ca + Na + K impurity content level objective of less than 0.04 wt. % and the calcium impurity concentration was reduced by factors from over 5 for lot 9-4 to over 31 for lot 9-5. Lot 9-2 came close to meeting these objectives and lot 9-3 met the total Ca objective, but had high concentrations of Na and K. The iron concentrations of lots 9-4, 9-5, and 9-6 were also disappointingly high and were the result of comminution processing on the part of the supplier. The O,C analyses were reasonably consistent with the exception of lots 9-3 and 9-4.

Figure 1 provides a manufacturing flow sheet for Lot 1 produced from Si powder Source A. Lot 2 was produced in a similar fashion except that

Table 1. SPECTROCHEMICAL ANALYSIS OF Si_3N_4 POWDER LOTS

		Improved Lots					
	AME-8	AME 9-1	9-2	9-3	9-4	9-5	9-6
Wt. % Fe	0.170	0.035	0.065	0.065	0.15	0.330	0.210
Ca	0.250	0.030	0.040	0.030	0.048	0.008	0.025
Mg	0.015	0.005			0.002	0.006	0.005
Al	0.500	0.060	0.120	0.300	0.064	0.100	0.080
Ti	0.010	0.030			<0.020	<0.020	<0.010
Mn	0.008	0.002			0.004	0.010	0.003
Na	0.0026	0.0012	0.0011	0.0210	<0.005	<0.005	<0.006
K	0.0054	0.0025	0.0034	0.0580	<0.029	<0.005	<0.0010
(Ca+Na+K)	0.2580	0.0337	0.0445	0.1090	0.082	0.018	0.032
O	1.9*	1.65	1.63	2.38	1.71	1.41	1.34
C	0.26*	0.25	0.24	0.22	0.22	0.18	0.18
Moisture		0.01	0.02	0.85	0.94	0.03	0.03

**

*Analyses performed by M.I.T

**Analyses on lots 1-6 performed at NASA/Lewis Research Center by inert gas fusion technique for oxygen and by induction heating-chromatographic finishing technique for carbon.

Table 2. X-RAY ANALYSIS OF Si_3N_4 POWDER LOTS

Phase Lot	AME-8	AME 9-1	9-2	9-3	9-4	9-5	9-6
α Si_3N_4	85	77	77	83	91	88	87
β Si_3N_4	15	23	23	17	9	12	13
Si_2N_2O	trace	trace	trace	none	none	wk.trace	none
Fe Silicides	none	none	none	none	none	none	none

Figure 1. Lot 1 Flow Sheet

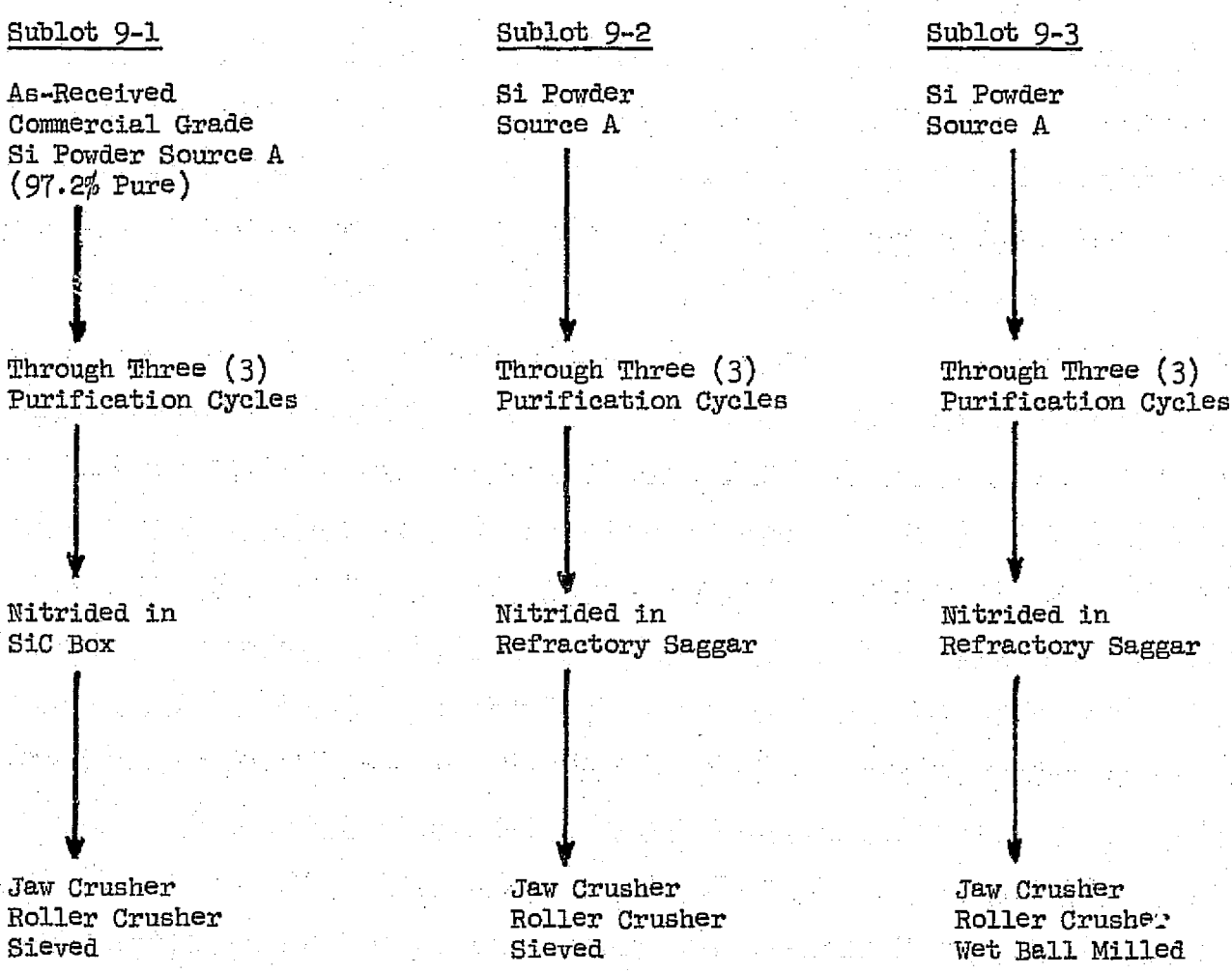

Si powder source B was employed. The high Na and K concentrations (Lot 9-3) resulted from the wet ball milling operation employing ceramic media which was discontinued.

Consolidation and Characterization - Samples were consolidated by standard hot pressing techniques. The conditions and results are reported in Table 3. The billet size was approximately 7.6 cm (3") dia. by 2.54 cm (1") thick.

The initial fabrication runs involved use of mainly AME Controlled Phase Grade (AME 8) Si_3N_4 powder in a series of experiments employing densification additives other than MgO. These additives were originally selected to improve the elevated temperature properties of Si_3N_4 by achieving a more refractory grain boundary phase without loss of impact strength. Judging by the high relative density achieved in run no. 1923, the CaO additive was effective as a densification aid. This was expected since the CaO - SiO_2 system is in many ways analogous to the MgO - SiO_2 system. MgO is an additive conventionally used in the densification of silicon nitride and it is believed to combine with the SiO_2 associated with the Si_3N_4 powder.[1] Further, since AME Supergrade Si_3N_4 powder already has at least 0.2 wt. % CaO, it was thought the addition of CaO might not be as serious a detriment to high temperature properties as the addition of MgO. This thought was based on the fact that the eutectic for the CaO-MgO-SiO_2 system is 1336°C (2437°F), while the eutectic for CaO-SiO_2 is 1436°C (2617°F), and MgO-SiO_2 is 1543°C (2809°F). The microstructure of this billet (1923) is shown in Figure 2. Little porosity is evident; however, the unidentified high reflectivity phase appears to be in greater evidence than previous pressings[2] conducted with 4 wt. % MgO additive. This may be more a result of the particular powder lot employed than the additive, however.

Run 1935 also employed AME Supergrade Si_3N_4 powder which is approximately 65% β Si_3N_4 and 35% α Si_3N_4. This billet with 1 wt. % MgO additive densified readily, reaching essentially 100% of theoretical density in the standard pressing cycle. The structure of this billet is shown in Figure 3. Regions up to 90 µm of an unidentified second phase are apparent. The phase is preferentially aligned normal to the pressing direction. The large pores are thought to be regions which were occupied by the high reflectivity phase prior to removal during the polishing. This conclusion was reached upon observing portions of the phase bonded to the wall of one such cavity. Fe_3Si phase found in billets fabricated from AME 8 Si_3N_4 (85% α Si_3N_4) powder is more in the order of 5-15 µm in diameter. Based on second phase particle size, the use of Supergrade Si_3N_4 powder was discontinued in favor of AME-8 for the "control" powder.

Si_3N_4 billet 1949 was a second attempt to achieve a more refractory grain boundary phase. The additive was "Zyttrite" which is .05 µm particle size 6.5 mole percent Y_2O_3 stabilized ZrO_2. Greater than 99% of theoretical density was achieved demonstrating the effectiveness of this compound as a densification aid. The microstructure of billet 1949 is shown in Figure 4, and demonstrates a high density and the presence of additional phases. These phases in appearance are similar to those observed for the standard MgO additives, at the 1 and 4 wt. % levels. X-ray analyses did not reveal the presence of a phase resulting from the zirconia

Table 3. SILICON NITRIDE BILLET FABRICATION CONDITIONS AND RESULTS

Run No.	Material	Additive	Temp. °C	Temp. °F	Pressure MN/m^2	Pressure psi	Time min.	Density gm/cc	Phases by XRD	Grain Size (μm)
1923	Supergrade AME Si_3N_4	4 w/o CaO	1750	3182	27.5	4000	120	3.17		1.1
1935	Supergrade AME Si_3N_4	1 w/o MgO	1750	3182	27.5	4000	120	3.21		1.0
1949	AME-8 (Controlled Phase Grade)	4 w/o Y_2O_3 Stab. ZrO_2	1750	3182	27.5	4000	120	3.22		0.9
1963	AME 9-1	4 w/o MgO	1750	3182	27.5	4000	120	3.18	Iron Silicide	0.8
1966	AME 9-2	4 w/o MgO	1750	3182	27.5	4000	120	3.19	" "	0.9
1967	AME 9-3	4 w/o MgO	1750	3182	27.5	4000	120	3.17	" "	0.9
1954	AME-8	4 w/o Y_2O_3	1750	3182	27.5	4000	120	3.23		0.9
1955	AME-8	4 w/o Al_2O_3	1750	3182	27.5	4000	120	3.14		1.0
1958	AME 9-1	1 w/o MgO	1750	3182	27.5	4000	120	3.14		
1969	AME 9-2	1 w/o MgO	1800	3272	27.5	4000	120	3.12		0.8
1970	AME 9-3	1 w/o MgO	1800	3272	27.5	4000	60	3.15		
1972	AME-8	4 w/o MgO	1750	3182	27.5	4000	120	3.15		1.0
1992	AME-8 Forged	4 w/o MgO + Avco CVD SiC Filaments	1750	3182	27.5	4000	120	3.18		

Table 3 (cont.)

Run No.	Material	Additive	Temp. °C	Temp. °F	Pressure MN/m^2	Pressure psi	Time min.	Density gm/cc	Phases by XRD	Grain Size (μm)
2086	AME 9-2 De-agglomerated	4 w/o ZrO_2 (Y_2O_3 stab.)	1750	3182	41.4	6000	120	3.23	Fe_3Si Si_2ON_2	.8
2088	Plessey Si_3N_4	4 w/o ZrO_2	1750	3182	41.4	6000	120	3.21	Si_2ON_2	.9
2089	Plessey Si_3N_4	1 w/o MgO	1750	3182	41.4	6000	120	3.19	Fe_3Si Si_2ON_2	.8
1974	AME-8 Si_3N_4 Forged	4 w/o MgO	1800	3272	27.5	4000	190	3.18	Si_2ON_2	1.0
1996	AME-8 Si_3N_4 Forged	4 w/o MgO	1750	3182	27.5	4000	190	Sample distorted with irregular density distribution	Si_2ON_2	
1999	AME-8 Si_3N_4 Forged	4 w/o MgO	1750	3182	27.5	4000	190	3.17	Si_2ON_2	0.9
1020	AME-8 Si_3N_4	4 w/o MgO	1750	3182	27.5	4000	120	3.19	Fe_3Si	1.0
1021	AME 9-2	4 w/o MgO	1750	3182	27.5	4000	120	3.20	Si_2ON_2	0.9
1025	AME 9-2	15 w/o ZrO_2	1750	3182	27.5	4000	120	3.34	Zr Oxynitride	0.8
1049	AME 9-4	4 w/o MgO	1750	3182	27.5	4000	120	3.18		0.9
1050	AME 9-4	1 w/o MgO	1750	3182	27.5	4000	120	3.17		
1053	AME 9-5	1 w/o MgO	1750	3182	27.5	4000	120	3.14		
1055	AME 9-5	4 w/o MgO	1750	3182	27.5	4000	120	3.19		0.8
1056	AME-8	4 w/o MgO + Avco CVD SiC Filaments	1550	2822	27.5	4000	120	2.95		

Table 3 (concl'd)

Run No.	Material	Additive	Temp. °C	Temp. °F	Pressure MN/m^2	Pressure psi	Time min.	Density gm/cc	Phases by XRD	Grain Size (μm)
1058	AME 9-4	4 w/o MgO	1750	3182	27.5	4000	120	3.18	Si_2ON_2	
1059	AME-8	15 w/o ZrO_2	1750	3182	27.5	4000	120	3.37	Zr Oxynitride	0.9
1060	AME 9-4	15 w/o ZrO_2	1750	3182	27.5	4000	120	3.37	" "	
1061	AME 9-4	1 w/o MgO	1750	3182	27.5	4000	120	3.16	Si_2ON_2	
1062	AME 9-5	1 w/o MgO	1750	3182	27.5	4000	120	3.17		
1063	AME 9-4	4 w/o MgO	1750	3182	27.5	4000	120	3.19		
1064	AME-8	15 w/o ZrO_2	1750	3182	27.5	4000	120	3.36	Zr Oxynitride, Fe_3Si	
1070	AME 9-6	4 w/o MgO	1750	3182	27.5	4000	120	3.20		0.8
1071	AME 9-6	1 w/o MgO	1750	3182	27.5	4000	120	3.18		
1122	AME 9-1 Forged	4 w/o MgO	1750	3182	27.5	4000	120	3.17	Si_2ON_2	1.0
1123	AME-8 Forged	4 w/o MgO	1750	3182	27.5	4000	120	3.16		

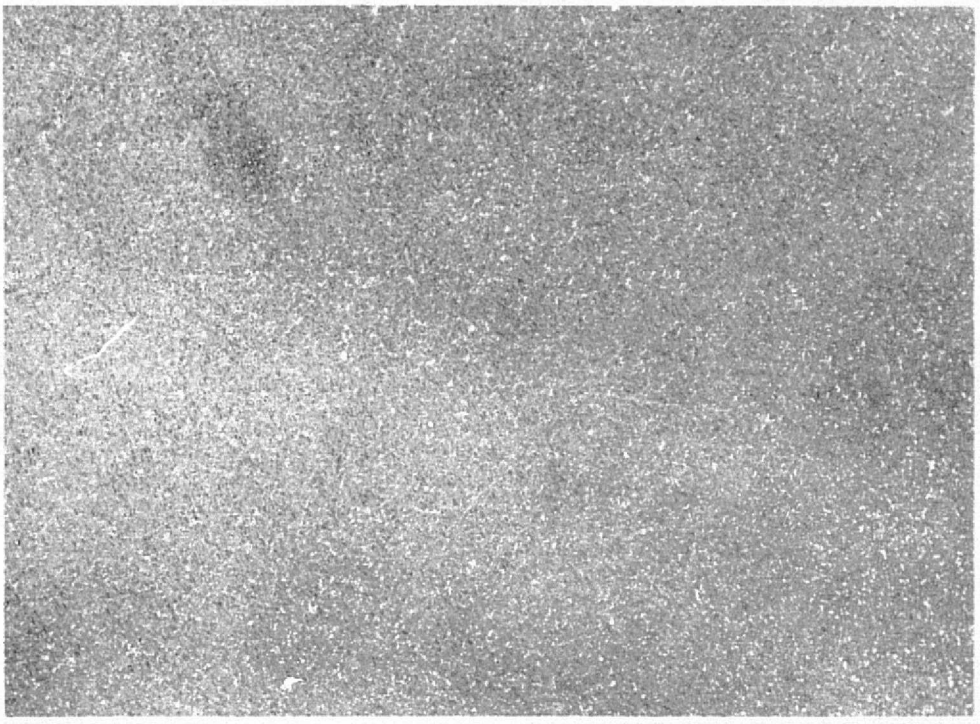

5798-1 100X

Figure 2. Microstructure of Billet 1923, AME Supergrade Si_3N_4 + 4 w/o CaO.

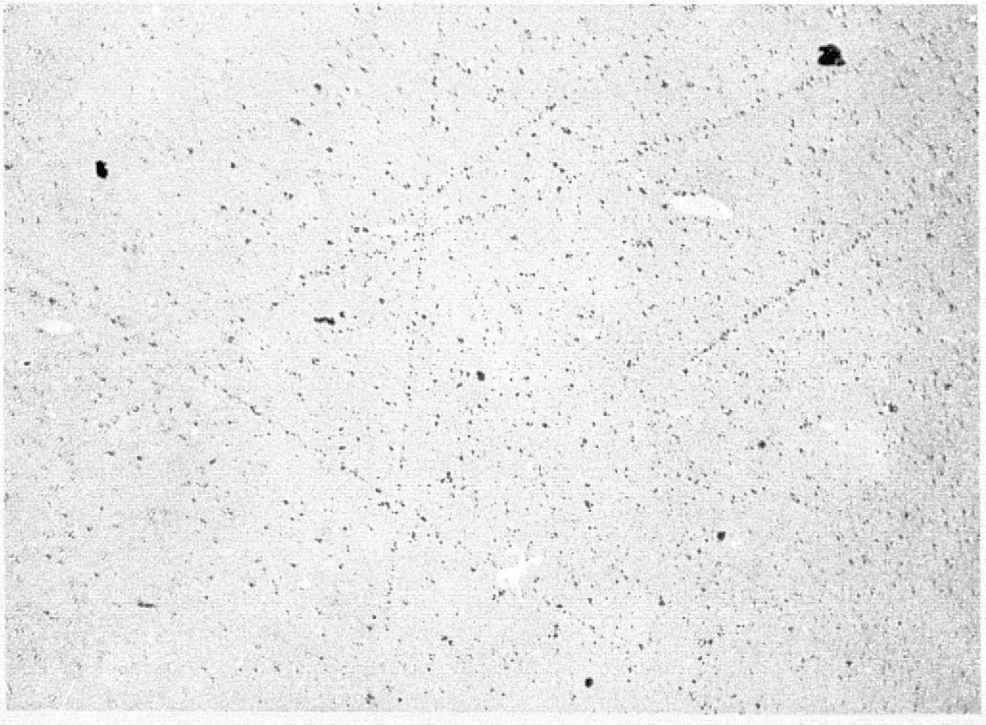

5823-2 100X

Figure 3. Microstructure of Billet 1935, AME Supergrade Si_3N_4 + 1 w/o MgO.

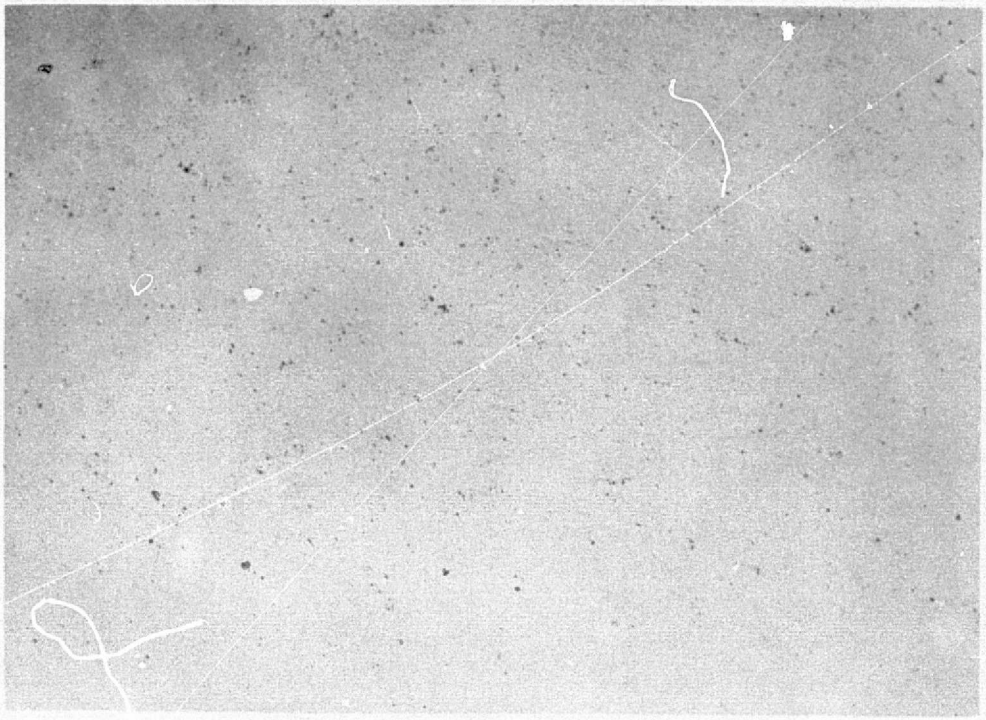

5836-2 (a) 100X

5836-1 (b) 500X

Figure 4. Microstructure of Billet 1949, AME-8 Controlled Phase Grade Si_3N_4 + 4 w/o ZrO_2.

additive. Only when the Zyttrite additive content reached 15 wt. %, as in billets 1025, 1059, 1060, and 1064, did X-ray analysis reveal the appearance of what has been tentatively identified as a zirconium oxynitride phase.

Y_2O_3 was added to Si_3N_4 for the preparation of billet 1954. This additive was demonstrated by Gazza[3] as an effective densification aid, and one that can result in good high temperature mechanical properties. The standard hot pressing cycle yielded a high density billet, and its microstructure is shown in Figure 5. The non-uniform porosity may have resulted from a non-uniform distribution of additive. Otherwise the structure is very similar to that of billet 1949 which contained the 4 wt. % ZrO_2 additive.

Si_3N_4 billet 1955 employed 4 wt. % Al_2O_3 as the densification aid. There were several reasons for implementing this additive--(1) the Al_2O_3-SiO_2 eutectic is 1595°C (2903°F), which is about 50° higher than the MgO-SiO_2 eutectic, and (2) the Al_2O_3 could react in situ forming the β' (sialon) phase which could be very refractory compared with the grain boundary phase in present materials. Structures wherein Al substitutes for Si and O substitutes for N in the Si_3N_4 structure are designated sialon compositions.[4] One possible negative aspect of an Al_2O_3 additive was that the Al_2O_3-CaO-SiO_2 eutectic is only 1170°C (2138°F) compared with 1336°C (2437°F) for MgO-CaO-SiO_2; thus, it does seem possible to end up with a less refractory grain boundary phase. Billet 1955, with a 3.14 gm/cc density, was prepared for evaluation and its microstructure is given in Figure 6. Here, the 4 wt. % Al_2O_3 addition resulted in a more uniform porosity than for billet 1954 (4 wt. % Y_2O_3) and less high reflectivity phase.

In the case of the MgO additions, both 1 and 4 wt. % were initially investigated. The one percent addition was chosen because prior stress rupture testing[2] demonstrated little advantage in lower MgO concentrations. Also noteworthy was the fact that comparative data was available in the earlier work involving Si_3N_4 with 1% MgO. Four (4) wt. MgO was also considered since earlier work also demonstrated that improved densities could be achieved in some powder lots with higher MgO concentrations. Further, comparative mechanical properties data also exist for this composition.

Billets 1963, 1966, and 1967 were each composed of one of the special grades of AME Si_3N_4 powder and 4 wt. % MgO additive. Microstructures of each of these billets are shown in Figures 7, 8, and 9. Analysis of these structures reveals limited porosity with scattered patches of a high index of refraction second phase material which has been identified as iron silicide (Fe_3Si).

The relatively high Na and K content in lot 9-3 precluded an extensive evaluation of this lot and in its place a cursory examination was performed on a Plessey Grade of high purity Si_3N_4 (overall purity was comparable to the AME special grades), as exemplified by billets 2089 and 2088. Microstructures of these billets are given in Figures 10 and 11. The Plessey sample with the 1% MgO additive (Billet 2089, Figure 10) reveals a dense microstructure with some apparent grain pull-out and scattered high index of refraction second phase material identified as Fe_3Si, as well as a

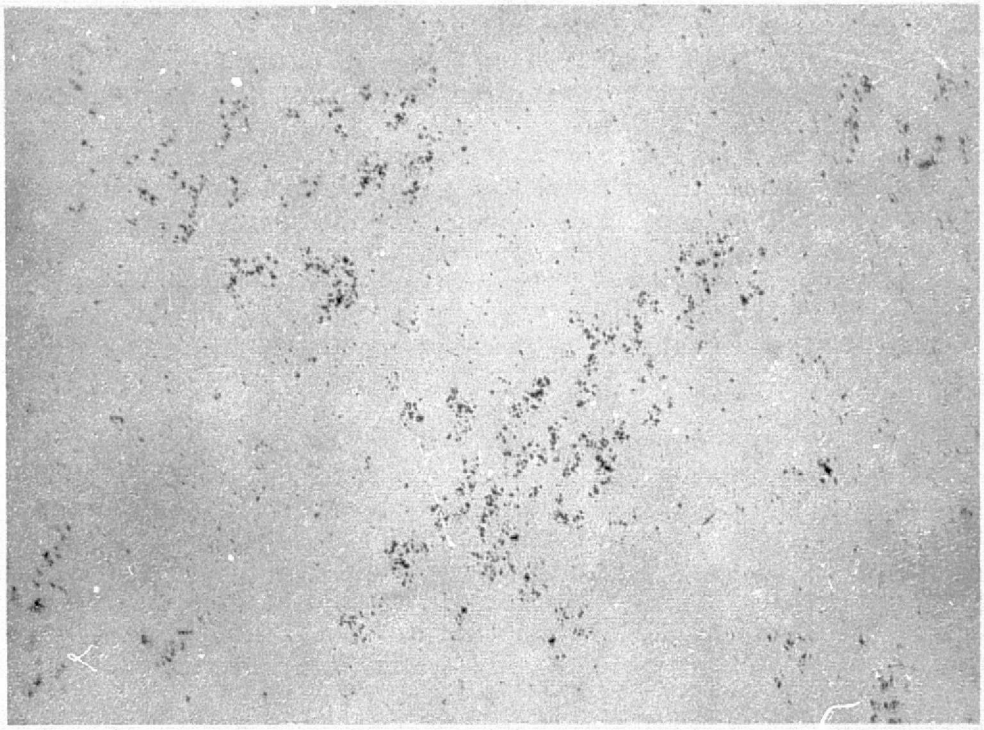

5842-1 (a) 100X

5842-3 (b) 500X

Figure 5. Microstructure of Billet 1954, AME-8 Si_3N_4 + 4 w/o Y_2O_3.

5842-2 (a) 100X

5842-4 (b) 500X

Figure 6. Microstructure of Billet 1955, AME 8 Si_3N_4 + 4 w/o Al_2O_3.

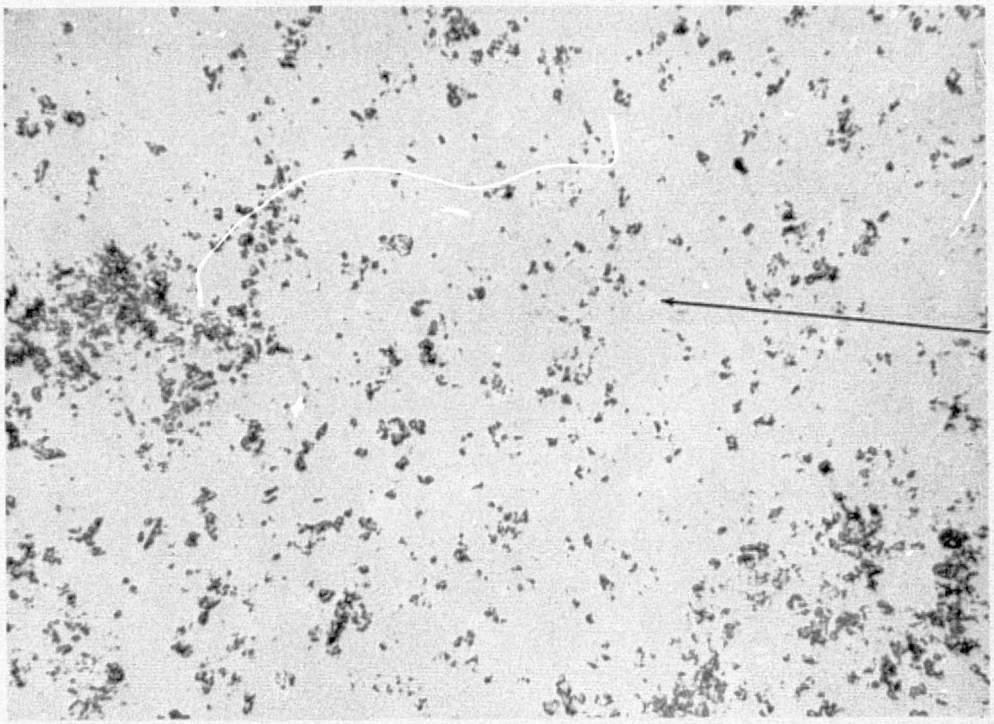

5852-3 500X

Figure 7. Microstructure of Billet 1963, 9-1 Si_3N_4 + 4 w/o MgO.

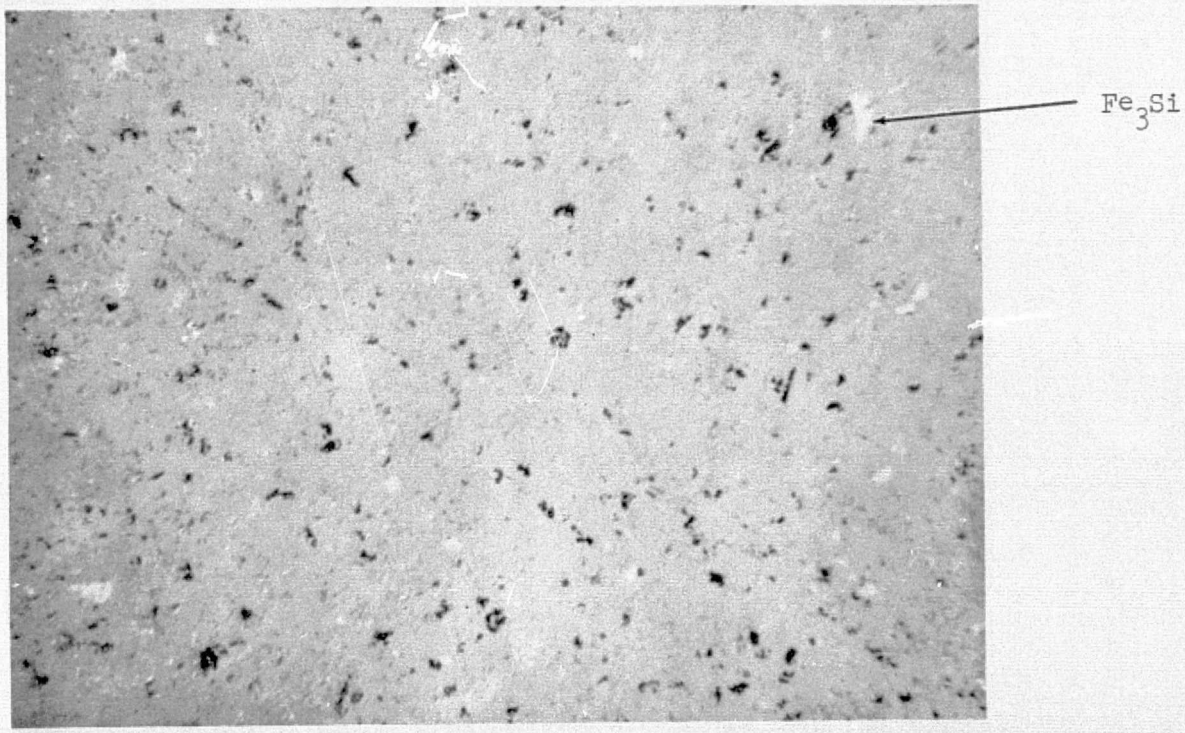

5849-9 500X

Figure 8. Microstructure of Billet 1966, 9-2 Si_3N_4 + 4 w/o MgO.

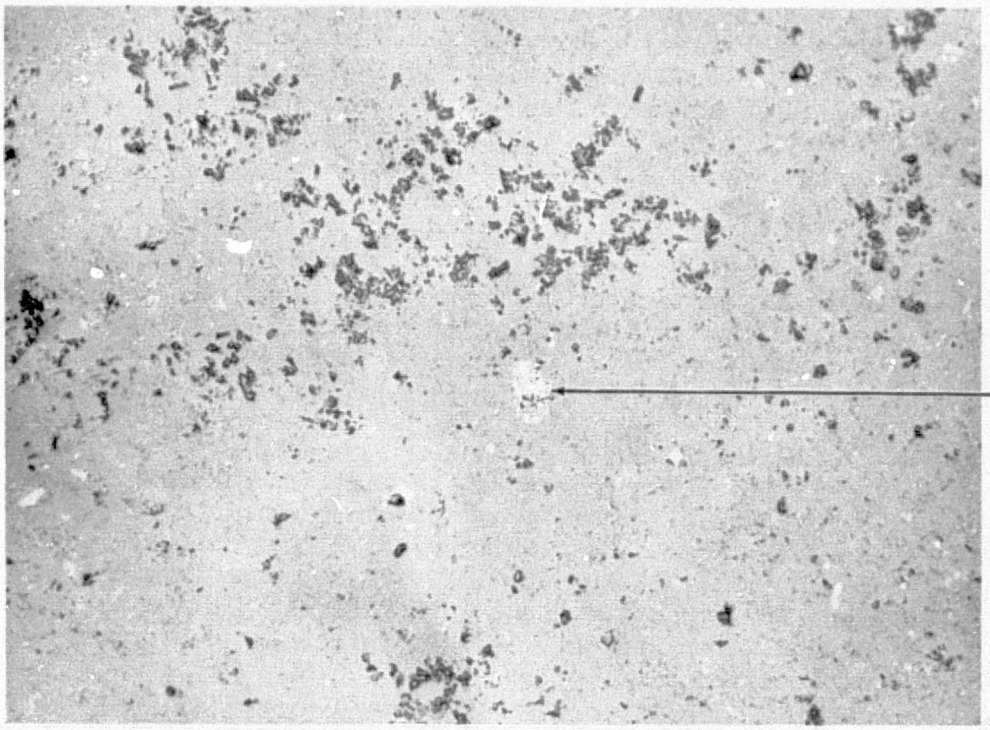

5849-3 500X

Figure 9. Microstructure of Billet 1967, 9-3 Si_3N_4 + 4 w/o MgO.

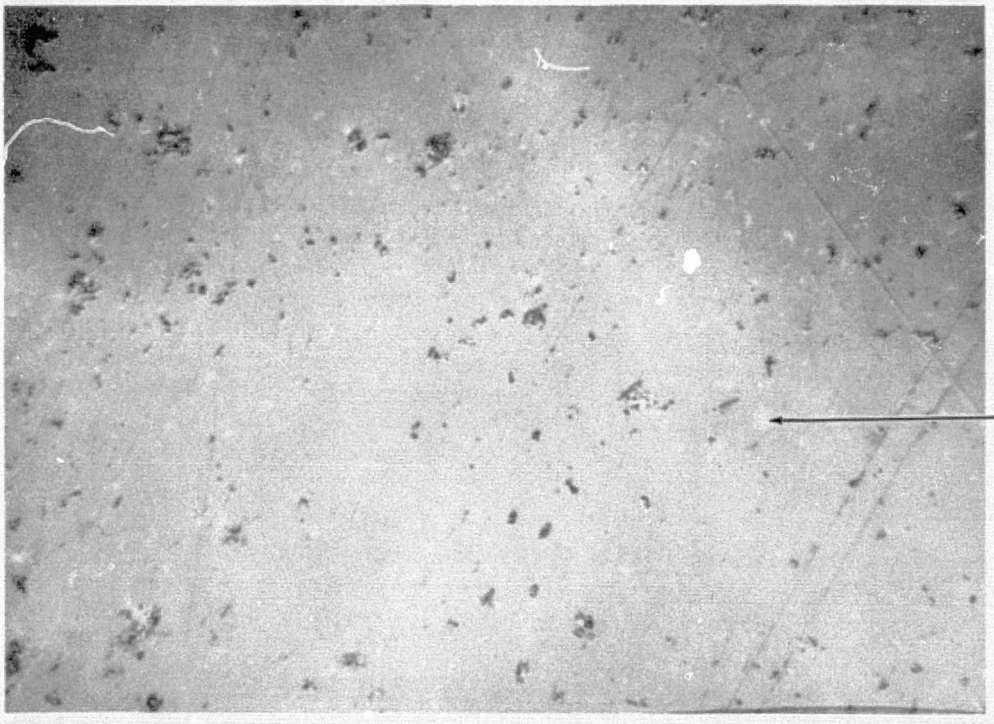

5901-1 500X

Figure 10. Microstructure of Billet 2089 Plessey Grade Si_3N_4 + 1 w/o MgO.

quantity of lower index (gray appearing) phase material suspected of being Si_2N_2O. Figure 11 (Billet 2088) shows a Plessey grade sample with 4 wt. % ZrO_2 additive and shows a higher concentration of the gray phase. An AME 9-2 grade material with 4 wt. % ZrO_2 additive, as exemplified by the microstructure of Billet 2086 in Figure 12, reveals more of the gray phase as well as the Fe_3Si phase.

The material used in the preparation of this billet was air classified to remove agglomerated particulates larger than 10 μm. It was thought that this treatment would provide a more uniform material and reduce the scatter of test results. This, in fact, was observed as is described below in a later section.

Examples of the microstructures obtained when 15 wt. % zyttrite additions were made are given in Figures 13 and 14. Figure 13 shows the polished section structure for billet 1059, composed of AME-8 source material and Figure 14 shows the structure for billet 1060, composed of AME 9-4. The microphotograph for the 1059 billet shows considerably more of the Fe_3Si phase than that for the 1060 billet as might be expected on the basis of original iron content. More detailed microstructure examination of these compositions is required to positively characterize the phase structure and chemistry of other apparent phases; however, iron silicide and oxynitride phases appear evident by polished section inspection.

Billets 1974, 1996, and 1999 were prepared by press forging pre-compacted cylindrical specimens in a graphite die whose internal diameter was approximately 1-inch larger than the compact diameter. The application of pressure and temperature to the specimens allowed densification to occur with lateral flow of material as in upset forging of metals. With appropriate rates of pressure application, generally intact specimens were produced. Porous peripheral regions of the forged specimens gave the appearance of possessing more of the silicon oxynitride phase which may be specific for the process conditions selected.

An attempt was also made to incorporate Avco chemically vapor deposited SiC filaments (.002 μm (.005 in.) dia.) into a matrix of hot pressed silicon nitride as in billet 1992. It was thought that the introduction of such high strength refractory filaments could enhance the impact resistance of the Si_3N_4 matrix through a crack interruption process. Examination of the fabricated composite did reveal filament-matrix interaction with some obvious filament degradation and the system received only minor emphasis in evaluation.

Silicon Carbide

Powder - Pittsburgh Plate Glass Co. high purity fine particulate (~.1 μm) β silicon carbide was obtained for this investigation. Characteristics of the SiC powder are given below in Tables 4 and 5.

Table 4. Carbon and Oxygen Contents for PPG Powder

Lot No.	% O_2	% Free Carbon	% Total Carbon
PPG-2	0.19	0.9	30.8

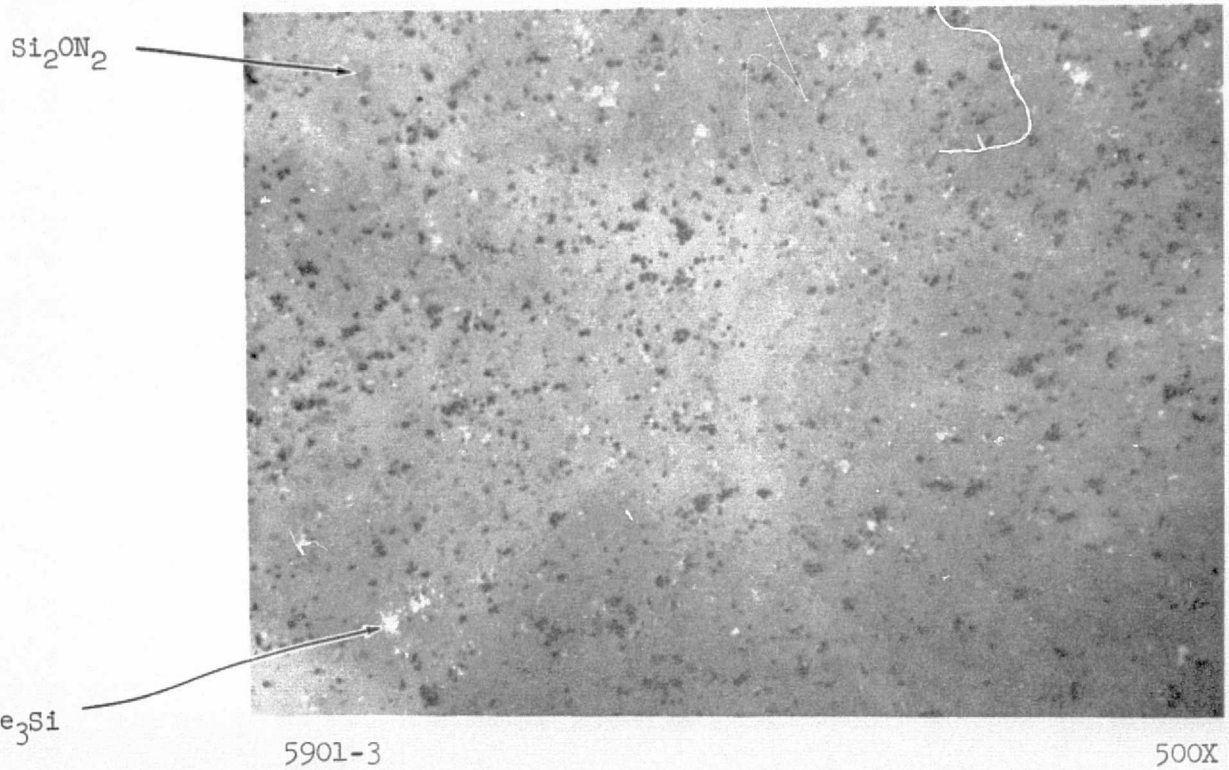

5901-3 500X

Figure 11. Microstructure of Billet 2088 Plessey Grade Si_3N_4 + 4 w/o ZrO_2.

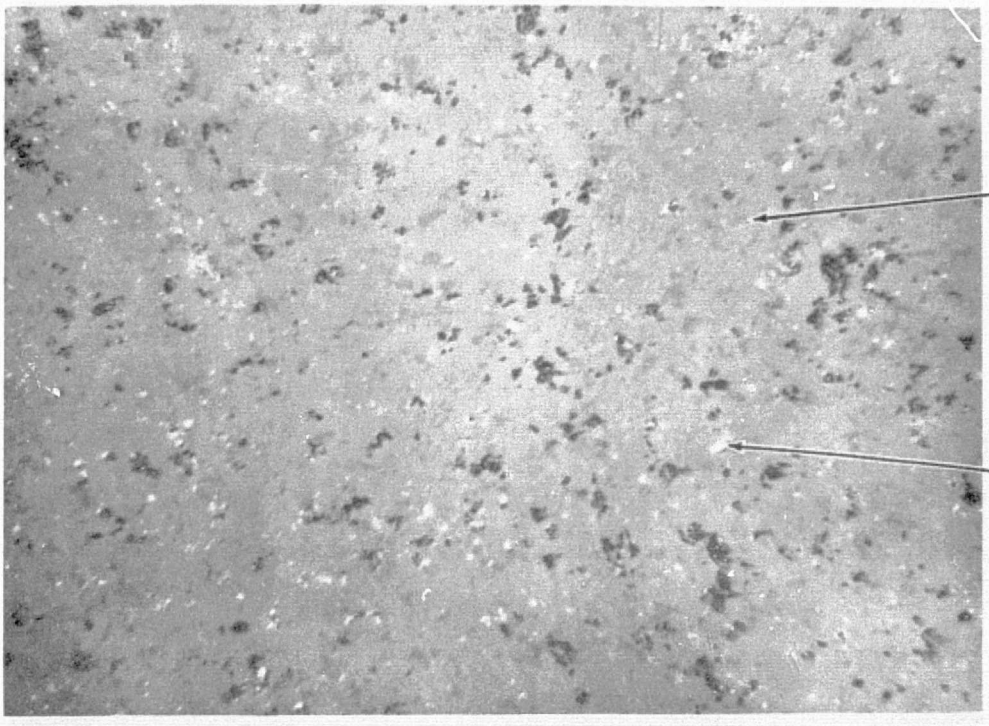

5901-2 500X

Figure 12. Microstructure of Billet 2086, AME 9-2 Si_3N_4 + 4 w/o ZrO_2.

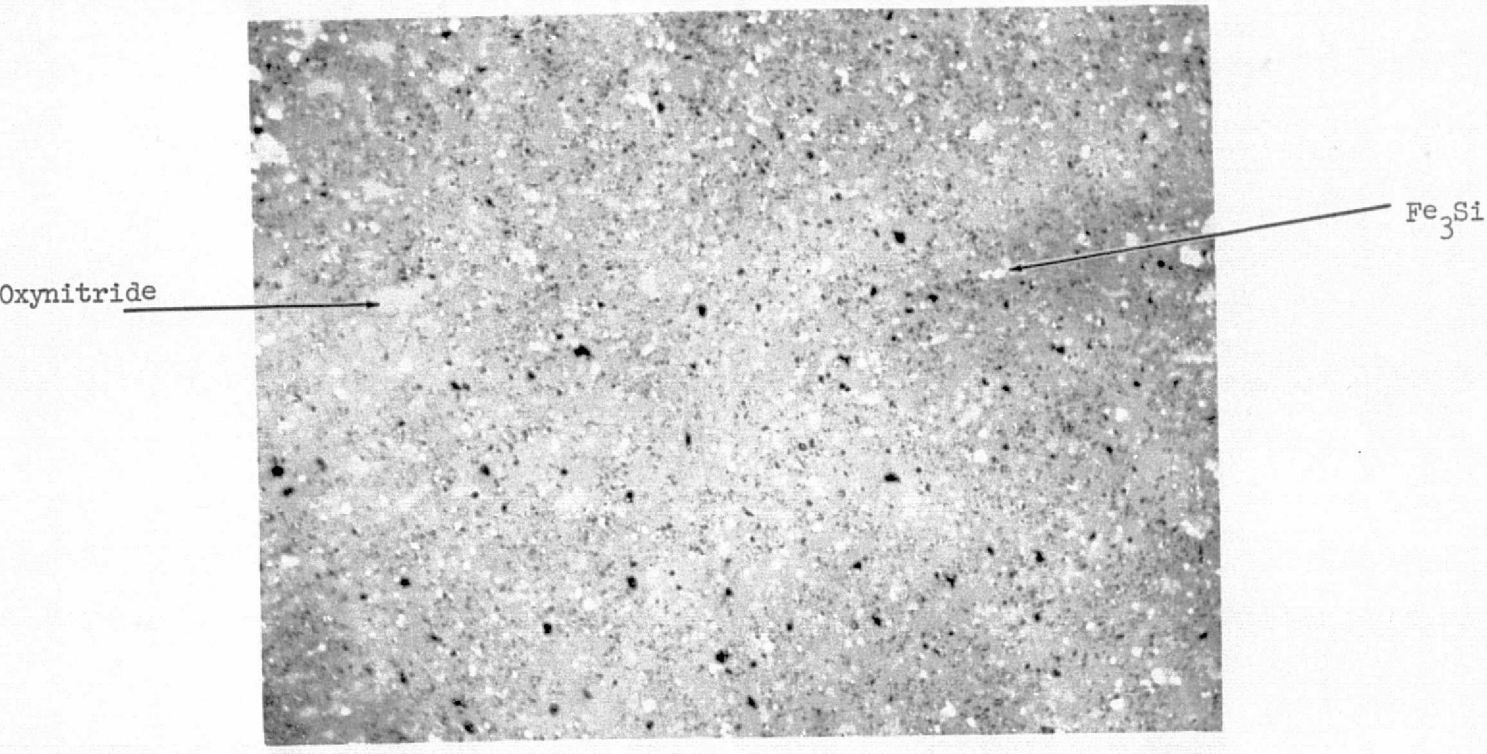

500X

Figure 13. Microstructure of Billet 1059 Composed of AME-8 with 15 w/o Zyttrite.

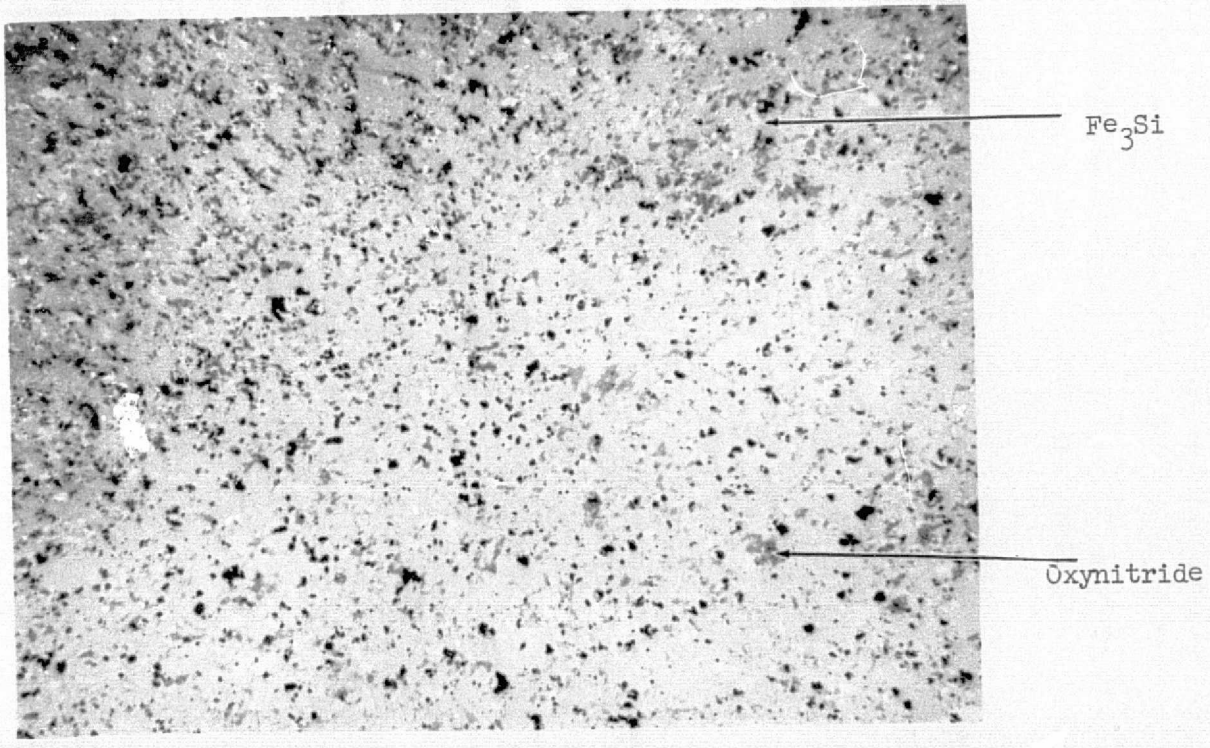

500X

Figure 14. Microstructure of Billet 1060 Composed of AME 9-4 with 15 w/o Zyttrite.

Table 5. Spectromchemical Impurity Analyses of SiC Lots

(Conc. in ppm)

Element/Lot	SiC #2
Ag	500
Al	100
B	1000
Ba	<100
Ca	<100
Cr	<100
Cu	500
Fe	1000
K	<1000
Mg	100
Mn	100
Na	<1000
Ni	< 100
Sr	<1000
Ti	1000

X-ray analysis revealed essentially pure β SiC powder with no other detectable phases. The PPG SiC powder was screened through 325 mesh to eliminate any large agglomerates or foreign particles.

Consolidation and Characterization

The fabrication conditions and results for the PPG powder are given in Table 6. Again, the billet sizes were 7.6 cm (3") dia. x 2.54 cm (1") thick.

The first billet (1945) was consolidated under a thermal cycle somewhat lower than employed in a previous program[2] for a 27.5 MN/m^2 (4000 psi) pressing pressure. The objective was to find the minimum conditions required to achieve high density and also provide a billet suitable for stress rupture testing. The billet was 99% dense; however, the microstructure as shown in Figure 15 exhibits marked secondary grain growth. This problem was also encountered on the previous program[2]. It was thought that correcting this through adjustment of the thermal cycle would be difficult and that increased carbon additions for retarding grain growth should be attempted. For Billet 1965, the amount of C was increased from $1\frac{1}{2}$ to 3 wt. %. The increased C concentration was thought to be sufficient to pin grain boundaries and prevent abnormal growth. Further, SiC pressing 1968 was run with a 2% BN addition, also for the purpose of avoiding abnormal needlelike grain growth. The run temperature for 1968 was reduced by 100°C (180°F). In both cases, densities of 3.12 g/cc were achieved, but were still coupled with a significant amount of abnormal grain growth as shown in the microphotographs in Figures 16 and 17. This is thought to be triggered by the β to α transformation in SiC. It is also possible that undetected α phase SiC in the starting powder may act as nucleation sites for exaggerated α-SiC crystallite growth at the hot press temperature employed.

Further effort at densifying SiC with the absence of abnormal growth

Table 6. Silicon Carbide Billet Fabrication Conditions and Results

Run No.	Material	Additive	Temp. °C	Temp. °F	Pressure psi	Pressure MN/m^2	Time min.	Density gm/cc	Phases by XRD	Grain Size (μm)
1945	PPG SiC	1½ w/o Al_2O_3 1½ w/o C	2100	3812	4000	27.5	60	3.17	SiC	10 x 100
1965	PPG SiC	1½ w/o Al_2O_3 3 w/o C	2140	3884	4000	27.5	15	3.12	SiC	5 x 20
1968	PPG SiC	2% BN	2040	3704	4000	27.5	60	3.10	SiC	8 x 30
2080	PPG SiC	1½ % C 1½% Al_2O_3	1930	3506	8000	55	30	3.10	SiC	5

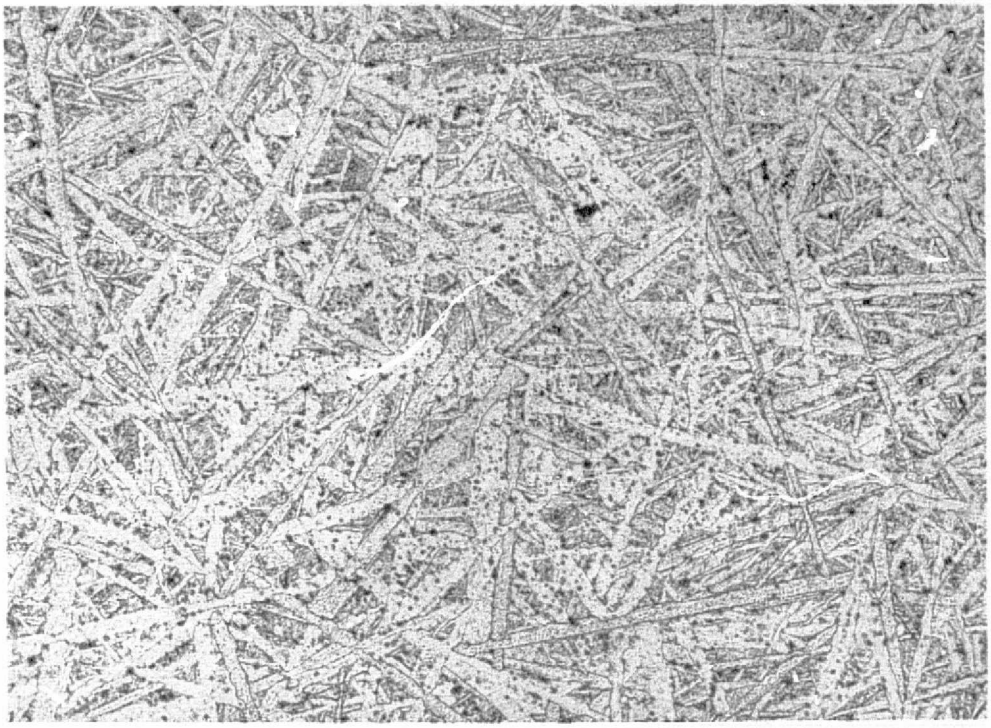

5835-4 100X

Figure 15. Microstructure of Billet 1945 Processed at 27.5 MN/m^2 (4000 psi), PPG SiC + $1\frac{1}{2}$ w/o Al_2O_3 and $1\frac{1}{2}$ w/o C.

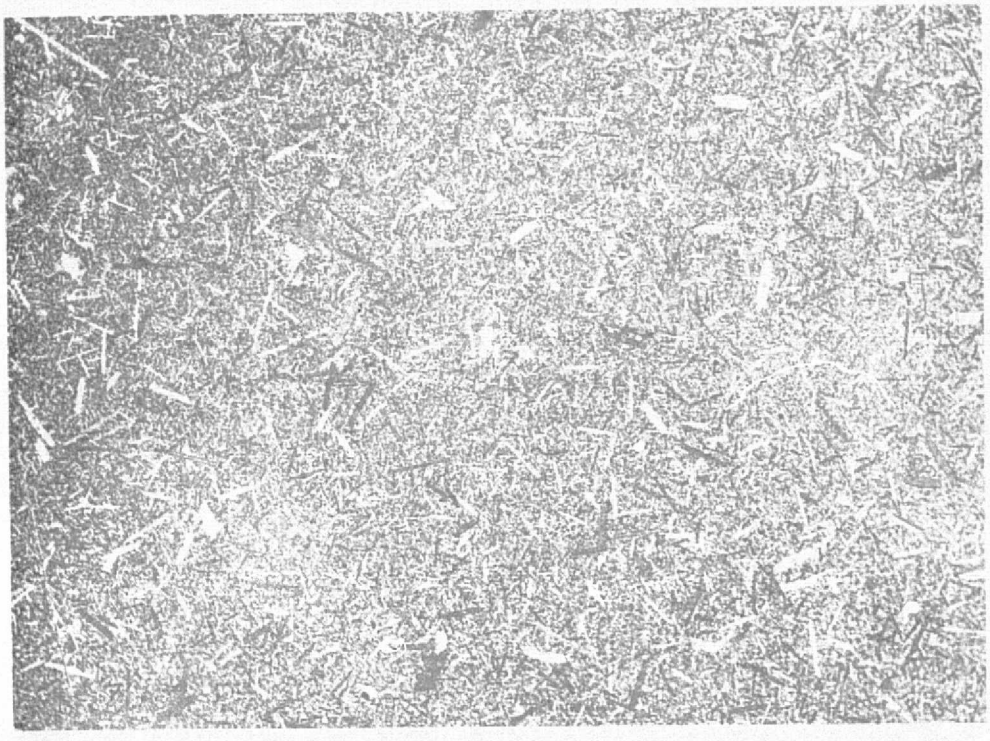

5850-4 100X

Figure 16. Microstructure of Billet 1965 Processed at 27.5 MN/m^2 (4000 psi), PPG SiC + 1½ w/o Al_2O_3 and 3 w/o C.

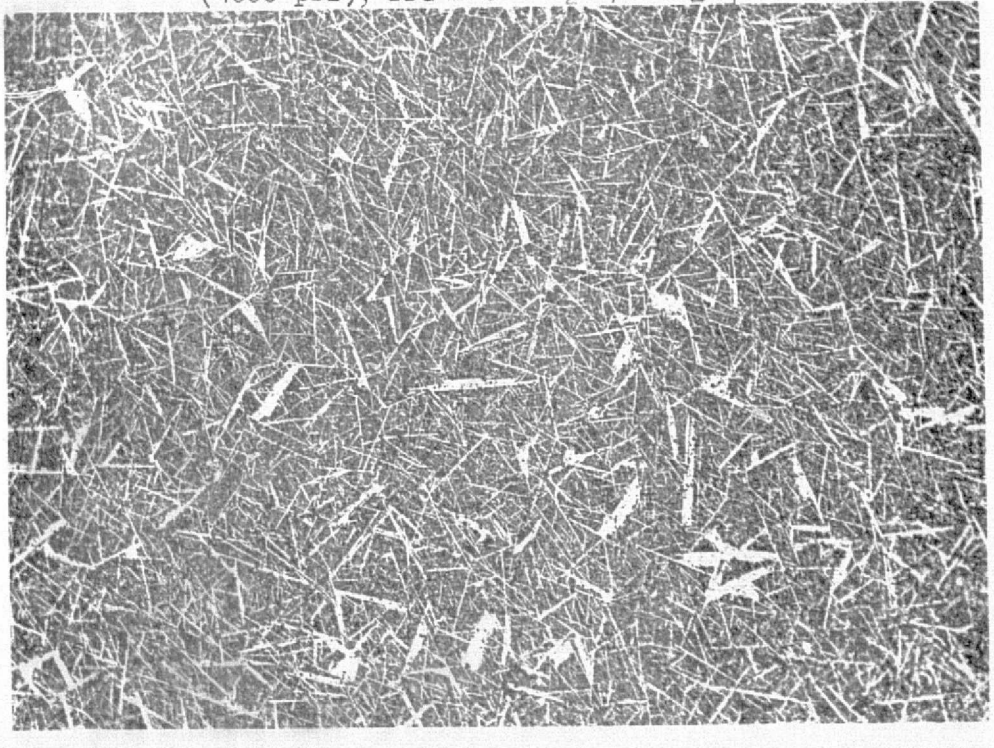

5849-8 100X

Figure 17. Microstructure of Billet 1968 Processed at 27.5 MN/m^2 (4000 psi), PPG SiC + 2 w/o BN.

proceeded along the lines of higher pressure hot pressing at reduced temperatures. The result was Billet 2080 prepared at a temperature two hundred degrees F lower than Billet 1968, but at a pressure of 55 MN/m^2 (8000 psi). This specimen exhibited reasonable densification at 3.10 gm/cc and showed no needle-shaped grains in the microstructure. Figure 18 shows the microstructure of this billet after etching to reveal the grain geometry. The structure shows some second phase segregation (believed to be aluminum oxycarbide) along with some porosity. Most important, no abnormal grain growth was observed with the grain size estimated to be about 5 μm. This structure received most of the properties evaluation described in subsequent sections of the report.

MATERIALS EVALUATION

General

It is well recognized that SiC and Si_3N_4 and composites based on these matrices have sufficient thermal shock resistance and thermal-chemical stability for serious consideration in the turbine application. However, the mechanical shock resistance is lower than presently used nickel-base superalloy systems; e.g., B1900 has an impact strength of 12.2, 7.5, and 1.4 Joules (108, 66, and 12 in-lbs.) at 1093°C (2000°F), 1149°C (2100°F), and 1260°C (2300°F), respectively[5], whereas the highest impact strength measured (same conditions) for a SiC or Si_3N_4 base material was 1.1 Joules (9.5 in-lbs.) for Si_3N_4 with a $LiAlSi_2O_6$ surface layer[6]. It is recognized that the impact strength measurements include the complex interaction of a number of fundamental material properties as well as dynamic effects of specimen-fixture interaction. Consequently, the impact strength measurement did not permit as detailed an interpretive analysis as might be desired, but it served as a very real measure of progress toward the goal of sufficient mechanical shock resistance for the turbine application. It is difficult to say precisely what value of impact strength is required for this application. A short range goal of 0.7 Joules (6 in-lbs.) was established for this program.

After sufficient impact testing and bend testing were accomplished to establish a promising material system, stress rupture testing was begun to determine if the material system had sufficient long term strength behavior to be of interest and learn if there was a correlation between this behavior, impact strength, and microstructure.

Mechanical Shock Resistance

A Bell Telephone Laboratories type impact tester was modified to provide impact strength data at temperatures from room to 1316°C (2400°F)[5]. There is no standard test described for ceramic materials at elevated temperatures by ASTM. However, the modified instrument does conform to the requirements of specification D256 - Standard Method of Test for Impact Resistance of Plastics and Electrical Insulating Materials. The previous effort[6] provided comparison data of two superalloys; a nickel-base material - B1900, and a cobalt-base material - X40. The impact tester was modified to include some of the requirements of ASTM E23-66 - Standard Methods for Notched Bar Impact Testing of Metallic Materials. Specimens 0.635 cm x 0.635cm (0.25 in x 0.25 in) in cross-section, 5.50 cm (2.165 in) long with

5875-5 (a) 100X

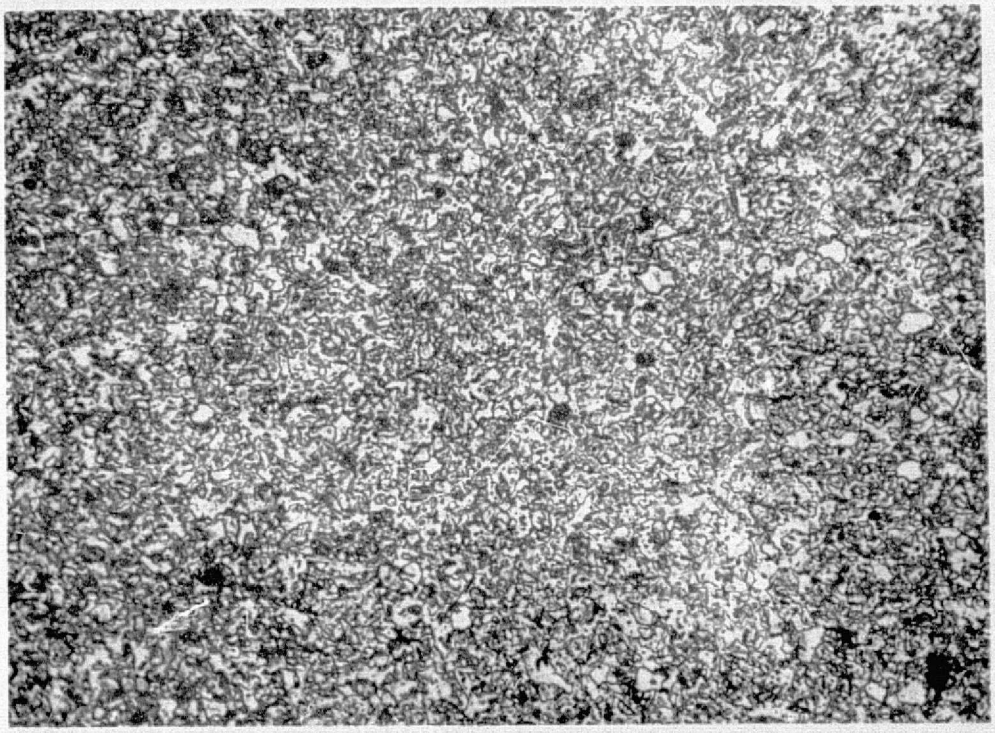

5875-4 (b) 500X

Figure 18. Microstructure of Billet 2080 Processed at 55 MN/m^2 (8000 psi), PPG SiC + $1\frac{1}{2}$ w/o Al_2O_3 and $1\frac{1}{2}$ w/o C.

a 4.00 cm (1.574 inch) gage length in a Charpy test mode were used. All the ceramic materials were unnotched and tested using a 2.7 Joule (2-foot pound) hammer while in the previous effort[5] a 21.7 Joule (16 foot-pound) hammer was used for the superalloys. Specimens were inserted into the hot furnace and soaked for 15 minutes prior to testing.

Impact strength measurements are reported in Tables 7, 8, and 9, and plotted in Figures 19, 20, 21, and 22. In general, three smaller size bars were tested at each of four temperatures, while larger cross-section bars 1.02 cm x 1.02 cm (.4" x .4") were tested at each of three temperatures.

Overall, the employment of the special purity grades of silicon nitride did not improve on the maxima in impact strengths observed in the effort of prior years[2,5,6]. However, the data do appear more consistent throughout a temperature range as shown in Figure 19. In the case of the higher purity silicon nitride, the results of testing of the larger cross-section bars do show some significant enhancement of impact resistance over bars made of standard controlled phase grade material as shown in Figure 20. This, too, is consistent over a temperature range. Of the additives employed, the ZrO_2 addition appears most effective and is consistent over a range of compositions.

Stereoscopic examination has revealed, in a number of instances, that failure initiation appears to occur from the site of inclusions. The data for Billet 2086 show the value of powder classification in providing consistent behavior with minimal data spread.

In very few instances was a value of ~0.7 Joules (6 in-lbs) achieved for the smaller sized test bars. These turned out to be in the case of hot forged samples. Each of three forged billets of AME controlled phase grade material (1972, 1905, and 1999) showed at least one sample with an exceptional impact value, e.g., .526 joules, .795 joules, and .737 joules, respectively. Developed texture is believed to account for these results; however, there is considerable inconsistency.

The limited data for silicon carbide are not particularly noteworthy, and appear to reflect the lower fracture surface energy inherent in silicon carbide materials[8].

Figure 21 provides a graphical summary of small bar impact data obtained for SiC samples produced and evaluated over a several year period. Samples from Billet 2020, produced in an earlier program, exhibited significantly better test results than samples from any of the other billets. The high density (3.23 g/cc) obtained without exaggerated grain growth by hot pressing at 1950°C and very high pressure (10 Ksi) probably are the significant reasons for these results. The other billets fall short either in terms of density or exaggerated grain growth or both.

Figure 22 plots data for both large and small size impact bars of two SiC compositions with different additives and processed differently. The data reveal an apparent advantage of th :N additive and resulting duplex structure even though the densities for the two billets are comparable.

Table 7. Impact Strength Results for Si_3N_4

Small Bars, 0.635 cm x 0.635 cm (0.25" x 0.25") Cross Section

Billet	Material	Additive	Impact Strength, Joules (in.lbs.) R.T.		1100°C (2012°F)		1200°C (2192°F)		1325°C (2415°F)	
1935	AME Super-grade	1 w/o MgO	.0774	(0.685)	.398	(3.52)	.481	(4.26)	.194	(1.72)
			.172	(1.52)	.284	(2.51)	.325	(2.87)	.329	(2.91)
			.218	(1.93)	.303	(2.68)	.343	(3.04)	.352	(3.12)
1963	AME 9-1	4 w/o MgO	.326	(2.89)	.363	(3.22)	.336	(2.97)	.346	(3.06)
			.307	(2.71)	.345	(3.06)	.373	(3.30)	.324	(2.87)
			.286	(2.62)	.405	(3.58)	.384	(3.40)	.336	(2.98)
1966	AME 9-2	4 w/o MgO	.343	(3.04)	.477	(4.23)	.410	(3.62)	.387	(3.42)
			.377	(3.32)	.438	(3.87)	.442	(3.91)	.477	(4.21)
			.392	(3.47)	.363	(3.21)	.362	(3.20	.450	(3.98)
2086	AME 9-2 Classified	4 w/o ZrO_2	.474	(4.20)	.462	(4.08)	.450	(3.98)	.480	(4.24)
			.465	(4.11)	.503	(4.45)	.477	(4.22)	.465	(4.11)
			.438	(3.87)	.473	(4.18)	.426	(3.77)	.413	(3.65)
1972	AME-8 Controlled Phase Grade Forged	4 w/o MgO	.304	(2.69)	.385	(3.40)	.297	(2.63)	.417	(3.69)
			.408	(3.62)	.476	(4.21)	.447	(3.95)	.526	(5.10)
			.465	(4.11)	.435	(3.85)	.363	(3.21)	.340	(3.01)
2089	Plessey	1 w/o MgO	.395	(3.49)	.201	(1.78)	.401	(3.55)	.424	(3.76)
2088	Plessey	4 w/o ZrO_2	.269	(2.38)	.304	(2.69)	.256	(2.26)	.35[illegible]	(3.11)
			.280	(2.48)	.288	(2.55)	.307	(2.71)	.2[illegible]	(1.77)
			.351	(3.11)	.325	(2.87)	.364	(3.22)	.319	(2.82)
1905 Ref. 7	AME-8 Forged	$\frac{1}{4}$ w/o MgO	.332	(2.94)	.795	(7.03)			.424	(3.75)
1999	AME-8 Forged	$\frac{1}{4}$ w/o MgO	.229	(2.03)	.463	(4.10)			.340	(3.01)
			.737	(6.60)	.419	(3.71)			.522	(4.61)
			.304	(2.69)	.385	(3.41)			.322	(2.85)

Table 7 cont.

Small Bars, 0.635 cm x 0.635 cm (0.25" x 0.25") Cross Section

Billet	Material	Additive	Impact Strength, Joules (in. lbs.) R.T.		1100°C (2012°F)		1200°C (2192°F)		1325°C (2415°F)	
1049	AME 9-4	4 w/o MgO	.253	(2.26)	.279	(2.47)	.279	(2.47)	.311	(2.75)
			.207	(1.83)	.330	(2.92)	.264	(2.34)	.331	(2.93)
			.228	(2.02)	.323	(2.85)	.296	(2.62)	.363	(3.21)
1059	AME-8	15 w/o ZrO_2	.332	(2.94)	.303	(2.68)	.356	(3.15)	.456	(4.03)
			.342	(3.04)	.329	(2.91)	.386	(3.42)	.436	(3.85)
			.307	(2.72)	.306	(2.71)	.397	(3.51)	.303	(3.68)
1060	AME 9-4	15 w/o ZrO_2	.333	(2.95)	.330	(2.92)	.343	(3.04)	.385	(3.41)
			.378	(3.35)	.343	(3.05)	.436	(3.85)	.400	(3.54)
			.356	(3.15)	.356	(3.15)	.371	(3.28	.336	(2.98)
1061	AME 9-4	1 w/o MgO	.425	(3.76)	.325	(2.87)	.300	(2.65)	.311	(2.75)
			.329	(2.91)	.198	(1.75)	.262	(2.32)	.364	(3.22)
			.262	(2.32)	.252	(2.25)	.350	(3.10)	.333	(2.95)
1062	AME 9-5	1 w/o MgO	.333	(2.95)	.329	(2.91)	.321	(2.84)	.333	(2.95)
			.301	(2.66)	.276	(2.45)	.264	(2.34)	.322	(2.85)
			.363	(3.21)	.325	(2.87)	.343	(3.05)	.363	(3.22)
1070	AME 9-6	4 w/o MgO	.233	(2.08)	.331	(2.93)	.266	(2.35)	.307	(2.72)
			.216	(1.91)	.299	(2.64)	.231	(2.06)	.255	(2.28)
			.263	(2.33)	.363	(3.21)	.250	(2.21)	.233	(2.08)
1071	AME 9-6	1 w/o MgO	.296	(2.62)	.352	(3.12)	.322	(2.85)	.300	(2.65)
			.175	(1.55)	.335	(2.97)	.251	(2.22)	.189	(1.67)
			.280	(2.48)	.322	(2.85)	.287	(2.54)	.276	(2.45)

Table 8. Impact Strength Results for Si_3N_4

Large Bars, 1.02 cm x 1.02 cm (.4" x .4") Cross Section

Billet	Material	Additive	Impact Strength, Joules (in.lbs.) R.T.		1100°C (2012°F)		1200°C (2415°F)	
1020	AME-8	4 w/o MgO	.917	(8.11)	.973	(8.61)	.942	(8.43)
			.880	(7.78)	.968	(8.56)	.918	(8.12)
			.892	(7.89)	.918	(8.12)	.875	(7.74)
1021	AME 9-2	4 w/o MgO	1.16	(10.27)	1.42	(12.6)	1.58	(14.0)
			1.14	(10.11)	1.25	(11.1)	1.29	(11.4)
			1.19	(10.5)	1.22	(10.8)	1.25	(11.1)
1049	AME 9-4	4 w/o MgO	1.27	(11.2)	1.33	(11.8)	1.60	(14.1)
			1.23	(10.9)	1.37	(12.1)	1.49	(13.2)
			1.19	(10.5)	1.31	(11.6)	1.45	(12.8)
1055	AME 9-5	4 w/o MgO	1.13	(9.95)	1.31	(11.6)	1.52	(13.4)
			1.17	(10.3)	1.35	(11.9)	1.39	(12.2)
			1.13	(10.0)	1.23	(10.9)	1.47	(13.0)
1070	AME 9-6	4 w/o MgO	.996	(8.91)	1.14	(10.1)	1.09	(9.67)
			.928	(8.21)	1.10	(9.74)	1.12	(9.92)
			1.06	(9.34)	1.27	(11.2)	1.22	(10.8)

Table 9. Impact Strength Results for SiC

Small Bars, 0.635 cm x 0.635 cm (0.25" x 0.25") Cross Section

Billet	Material	Additive	Impact Strength, in-lbs. (Joules) R.T.	1100°C (2012°F)	1200°C (2192°F)	1325°C (2415°F)
1968	PPG SiC	2% BN	.234 (2.072)	.213 (1.88)		.274 (2.42)
			.256 (2.270)	.189 (1.67)		.238 (2.11)
			.198 (1.75)	.250 (2.21)		.215 (1.90)
2080	PPG SiC	1½ w/o C	.123 (1.09)	.212 (1.87)	.105 (0.93)	.166 (1.47)
		1½ w/o Al_2O_3	.121 (1.07)	.239 (2.11)	.199 (1.76)	.238 (2.11)
			.172 (1.52)	.174 (1.54)	.174 (1.54)	.198 (1.75)

Large Bars, 1.02 cm x 1.02 cm (0.4" x 0.4") Cross Section

1968	PPG SiC	2% BN	.525 (4.65)	.645 (5.71)		.713 (6.31)
			.139 (12.30)	.474 (4.21)		.588 (5.20)
			.234 (2.07)	.690 (6.10)		.803 (7.11)
			.256 (2.27)			
2080	PPG SiC	1½ w/o C	.284 (2.51)	.425 (3.76)		.498 (4.41)
		1½ w/o Al_2O_3	.432 (3.82)	.464 (4.11)		.566 (5.01)

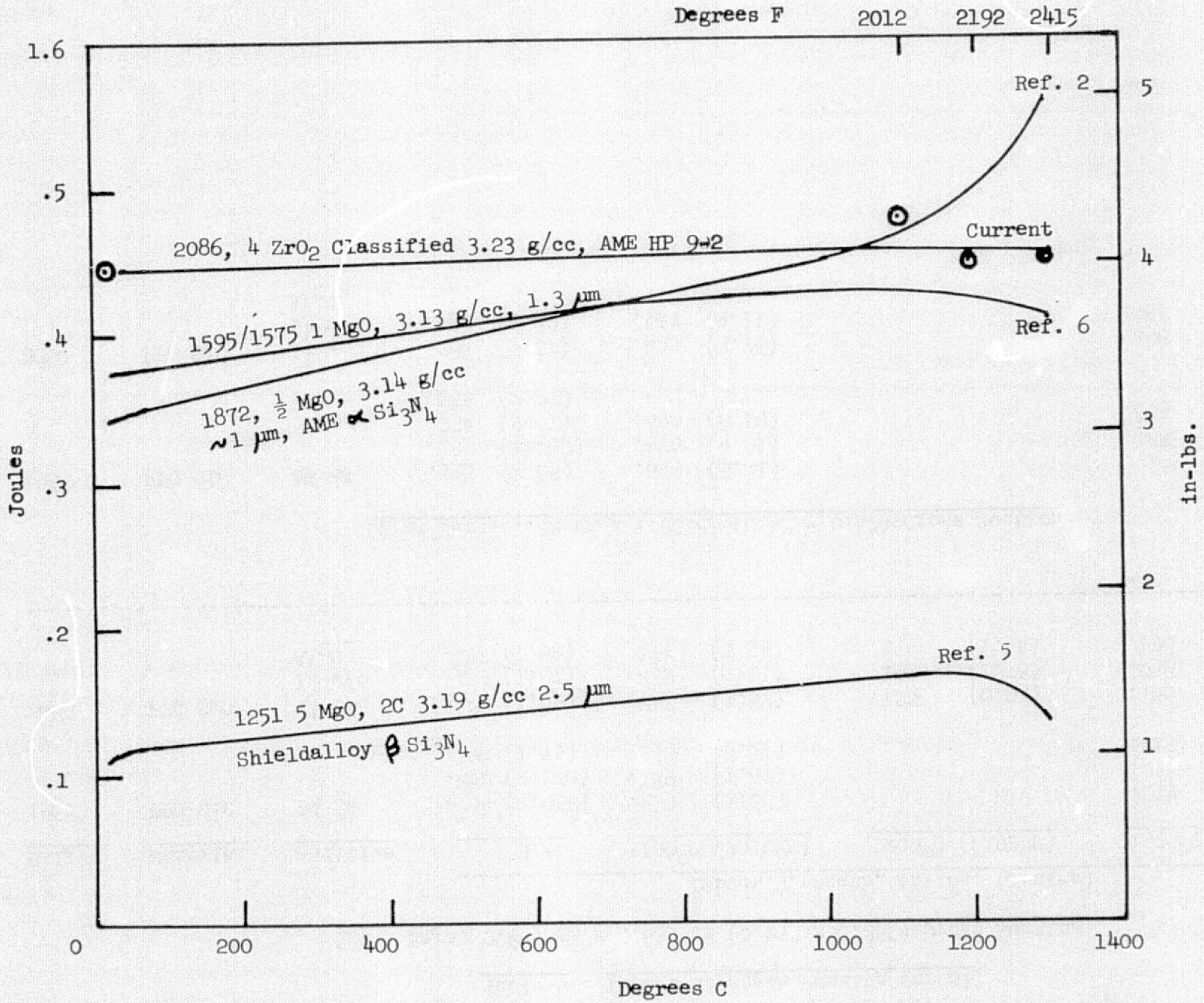

Figure 19. Small Bar Impact Resistance Measurements for Selected Silicon Nitride Compositions Comparing Results with Prior Investigations.

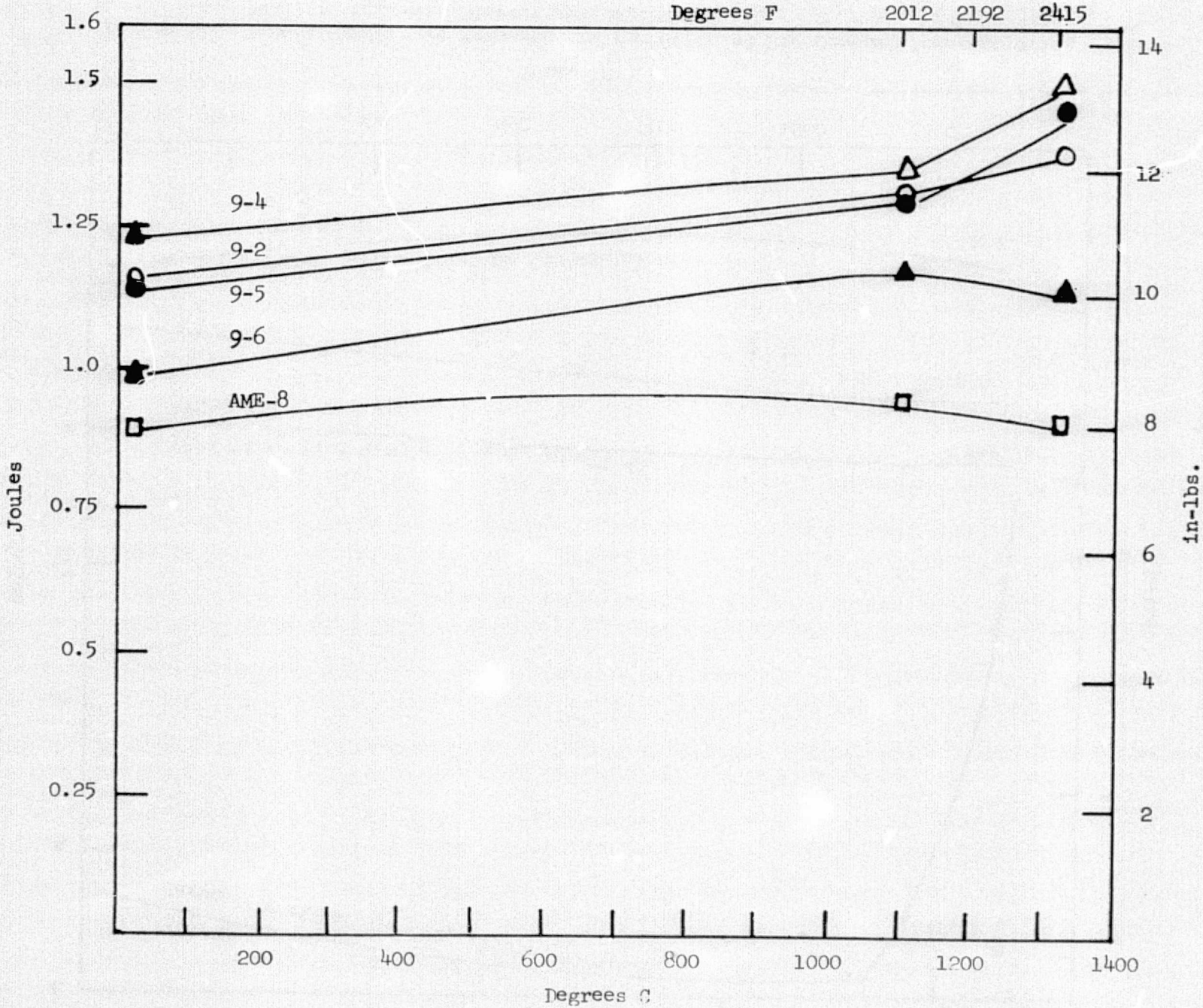

Figure 20. Impact Resistance Measurements on Larger Bars for Various Silicon Nitride Compositions each Containing 4 w/o MgO Additive.

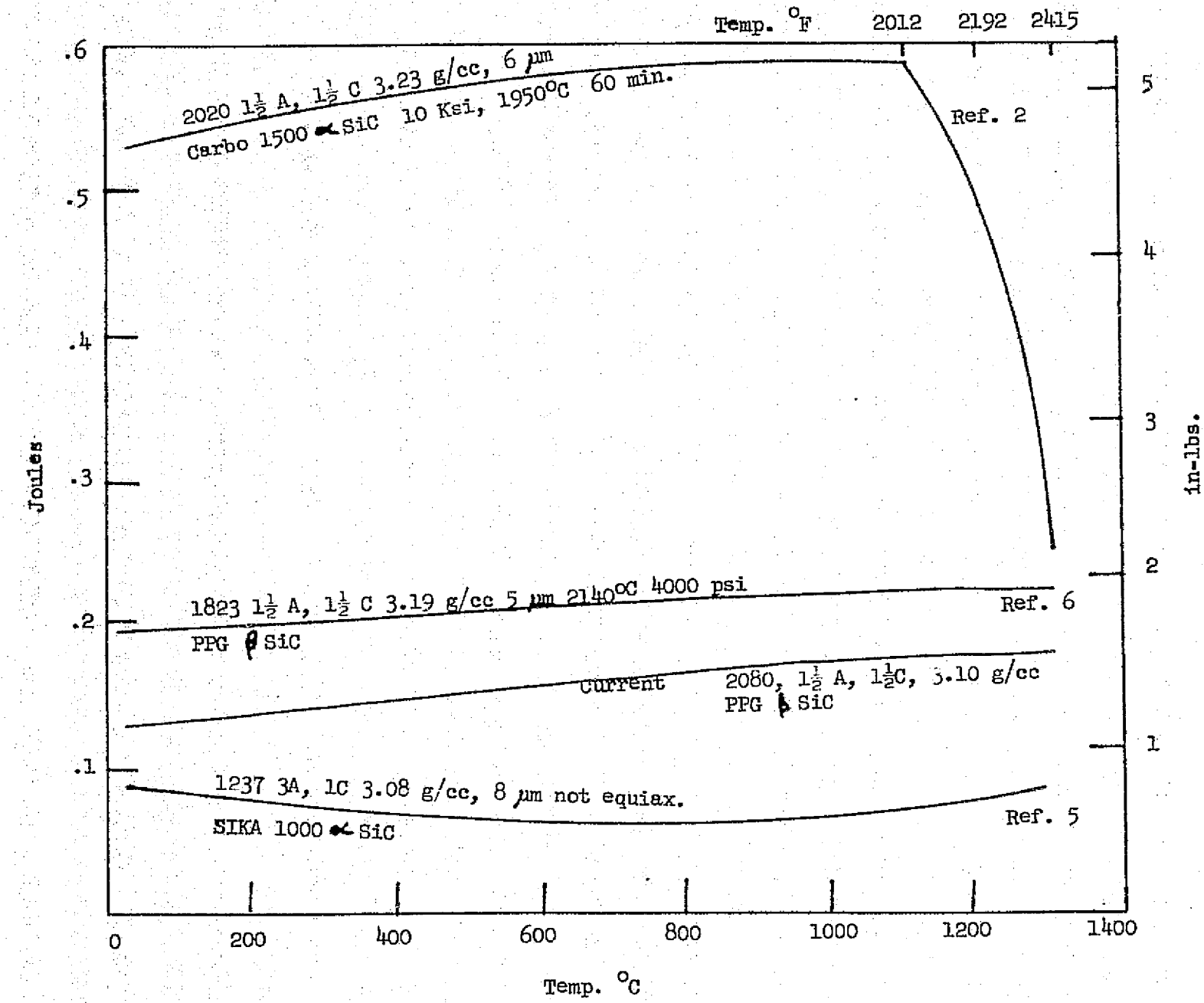

Figure 21. Impact Resistance Measurements for Selected SiC Compositions Comparing Results with Prior Investigations.

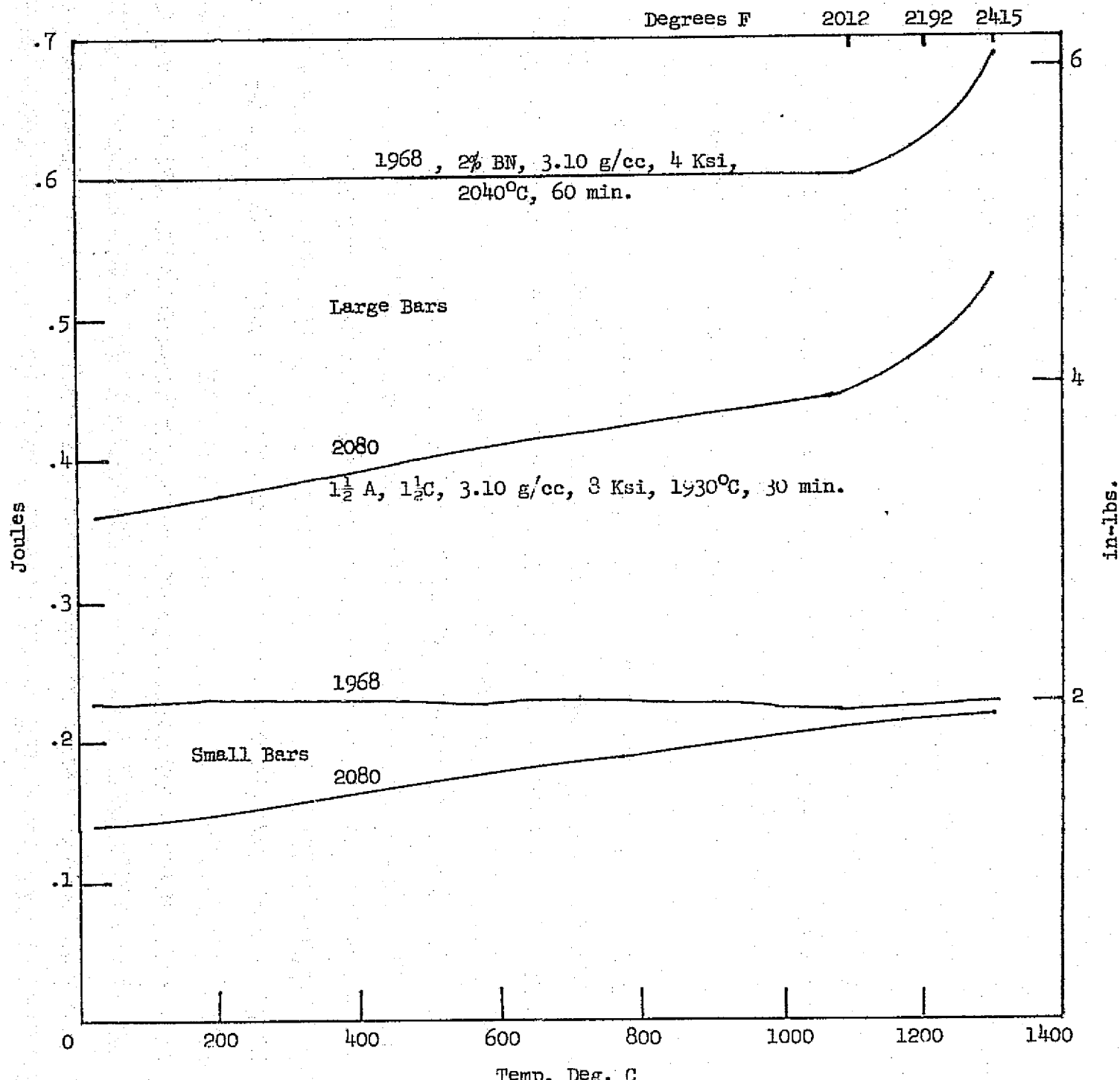

Figure 22. Impact Resistance Measurements for Large and Small Bar Air Sample Taken from the Same Billet Source Powder but Processed Differently.

Transverse Bend Strength

Short time 4 point bend tests were performed in air on specimens 4.45 cm x 0.51 cm x 0.25 cm (1 3/4" x .2" x .100") with an outer knife edge span of 3.81 cm (1.50") and an inner knife edge span of 1.27 cm (0.50") to insure elastic bend conditions. A constant load rate was set to provide a nominal strain rate of about 10^{-4} sec^{-1}.

Tests were run on most of the fabricated billets to determine the effectiveness of additives and purity. The results are documented in Table 10 and reveal the influence of higher purity, particularly at the highest test temperature. For a group of billets with 4 wt. % MgO additive, Figure 23, the billet 1020, which is characteristic of a "standard controlled phase" grade sample, shows values about half as high at the highest test temperature as those for billets 1049 (9-4 sublot), 1055 (9-5 sublot), and 1070 (9-6 sublot), and somewhat less than half as high as those for billets 1963 (9-1) and 1966 (9-2). The high Na and K content in lot 9-3 no doubt accounts for the low strengths observed at the highest test temperature for billet 1967. The billet 1923 (AME Supergrade Si_3N_4 powder) with the Ca additive showed the lowest values at 1325°C (2415°F). The Y_2O_3, Al_2O_3, and ZrO_2 additives showed rather promising results as additives to standard controlled phase grade material in tests at room temperature and 1325°C (2415°F) as shown in Figure 24. In particular, the ZrO_2 additive samples exhibited good low as well as high temperature strengths. The effectiveness of low concentration ZrO_2 additives to silicon nitride was also reported recently by other investigators[9]. As for the 4 wt. % addition, a 5 wt. % ZrO_2 addition was found to be even more effective in standard controlled phase grade powder as shown in Figure 25 and even higher strengths were obtained with the specially prepared lots 9-2 and 9-4, also shown in Figure 25.

The improvements in high temperature strength can be understood on the basis of the development of a refractory second phase in the boundary regions of the structure. The improvement at room temperature is not so clearly understood, however. Microstructural examination suggests a diminution in the appearance of relatively large β silicon nitride grains, which could contribute to a reduction of potential failure onset sites.

Stress Rupture

Testing was conducted in air under a four point bending mode using SiC for knife edge fixtures. The specimens were 4.45 cm x 0.51 cm x 0.25 cm (1 3/4 x 0.100 x 0.200 inches) with an outer span of 3.81 cm (1.500 inches) and an inner span of 1.27 cm (0.500 inch). A pre-determined load was applied smoothly in a few seconds with a cam accuator on the load bearing lever arm. A cut-off switch-clock circuit connected to the lever arm was utilized to detect and record failure.

All of the results were analyzed using the elastic beam formula:

$$\sigma = \frac{3\,Pa}{bh^2}$$

Table 10. Transverse Bend Strength Results

Billet	Material	Additive	Bend Strength, MN/m^2 (Kpsi)							
			Room Temp.		1100°C (2010°F)		1200°C (2192°F)		1325°C (2415°F)	
1923	AME Supergrade Si_3N_4	4 w/o CaO	427.6	(62.2)					107.9	(15.7)
			380.9	(55.4)					134.1	(19.5)
			358.9	(52.2)					112.8	(16.4)
1949	AME-8 Controlled Phase Grade Si_3N_4	4 w/o ZrO_2	494.3	(71.9)					267.4	(38.9)
			499.8	(72.7)					237.2	(34.5)
			429.7	(62.5)					248.2	(36.1)
1954	AME-8	4 w/o Y_2O_3	579.6	(84.3)					215.9	(31.4)
			472.3	(68.7)					234.4	(34.1)
			442.8	(64.4)					209.0	(30.4)
1955	AME-8	4 w/o Al_2O_3	517.0	(75.2)					234.4	(34.1)
			468.9	(68.1)					198.0	(28.8)
			427.6	(62.2)					200.8	(29.2)
1963	AME 9-1	4 w/o MgO	489.5	(71.2)	468.9	(68.2)	317.6	(46.2)	225.5	(32.8)
			435.9	(63.4)	416.0	(60.5)	304.6	(44.3)	234.4	(34.1)
			488.1	(71.0)	455.1	(66.2)	297.0	(43.2)	248.2	(36.1)
1966	AME 9-2	4 w/o MgO	512.9	(74.6)	453.8	(66.0)	331.4	(48.2)	328.6	(47.8)
			393.3	(57.2)	486.8	(70.8)	278.4	(40.5)	215.2	(31.3)
			345.1	(50.2)	486.1	(70.7)	316.9	(46.1)	239.3	(34.8)
1967	AME 9-3	4 w/o MgO	418.7	(60.9)	417.3	(60.7)	214.5	(31.2)	144.4	(21.0)
			436.6	(63.5)	422.8	(61.5)	236.5	(34.4)	165.0	(24.0)
			368.5	(53.6)	415.3	(60.4)	193.2	(28.1)	170.5	(24.8)
1020	AME-8	4 w/o MgO	416.6	(60.6)	360.3	(52.4)	303.2	(44.1)	140.9	(20.5)
			400.1	(58.2)	382.3	(55.6)	266.1	(38.7)	193.9	(28.2)
			373.3	(54.3)	344.4	(50.1)	248.2	(36.1)	154.0	(22.4)
1049	AME 9-4	4 w/o MgO	383.6	(55.8)	477.8	(69.5)	461.3	(67.1)	365.1	(53.1)
			418.7	(60.9)	479.2	(69.7)	455.1	(66.2)	358.2	(52.1)
			427.0	(62.1)	455.1	(66.2)	433.8	(63.1)	347.2	(50.5)

Table 10 concl'd

Billet	Material	Additive	Bend Strength, MN/m^2 (Kpsi)							
			Room Temp.		1100°C (2010°F)		1200°C (2192°F)		1325°C (2415°F)	
1055	AME 9-5	4 w/o MgO	550.7	(80.1)	489.5	(71.2)	365.1	(53.1)	337.6	(49.1)
			542.5	(78.9)	435.9	(63.4)	356.1	(51.8)	332.1	(48.3)
			482.6	(70.2)	415.3	(60.4)	331.4	(48.2)	303.2	(44.1)
1064	AME-8	15 w/o ZrO_2	633.9	(92.2)	516.3	(75.1)	414.6	(60.3)	352.7	(51.3)
			612.6	(80.1)	455.1	(66.2)	374.7	(54.5	310.8	(45.2)
			564.5	(82.1)	428.3	(62.3)	353.4	(51.4)	303.2	(44.1)
1060	AME 9-4	15 w/o ZrO_2	676.5	(98.4)	585.8	(85.2)	533.2	(76.1)	427.0	(62.1)
			650.4	(94.6)	550.0	(80.0)	481.3	(70.0)	399.4	(58.1)
			520.1	(90.2)	509.5	(74.1)	427.6	(62.2)	387.8	(56.4)
1070	AME 9-6	4 w/o MgO	443.4	(64.5)	509.5	(74.1)	517.0	(75.2)	413.9	(60.2)
			408.4	(59.4)	467.5	(68.0)	490.2	(71.3)	396.0	(57.6)
			379.5	(55.2)	457.2	(66.5)	468.2	(68.1)	365.1	(53.1)
1025	AME 9-2	15 w/o ZrO_2	675.1	(98.2)	607.8	(88.4)	550.7	(80.1)	455.1	(66.2)
			661.4	(96.2)	564.5	(82.1)	517.0	(75.2)	406.3	(59.1)
			642.1	(93.4)	537.0	(78.1)	502.6	(73.1)	419.4	(61.0)

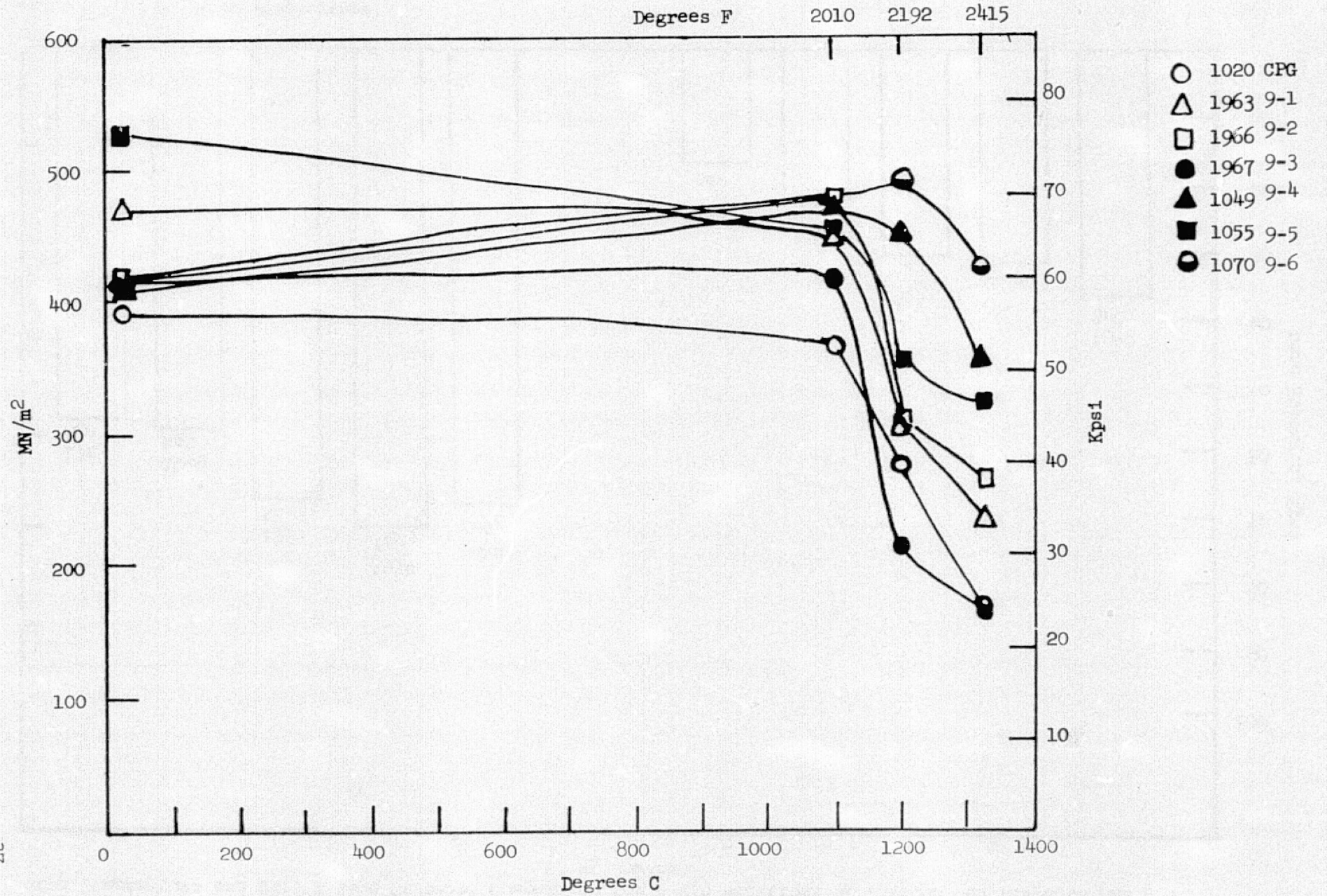

Figure 23. Bend Strength vs. Temperature Plots for Various Silicon Nitride Compositions each Containing 4 w/o MgO Additive.

Figure 24.

Room Temperature and 2415°F Bend Strength Comparison for 4 w/o Additions of Various Additives to AME CPG Si_3N_4 Powder

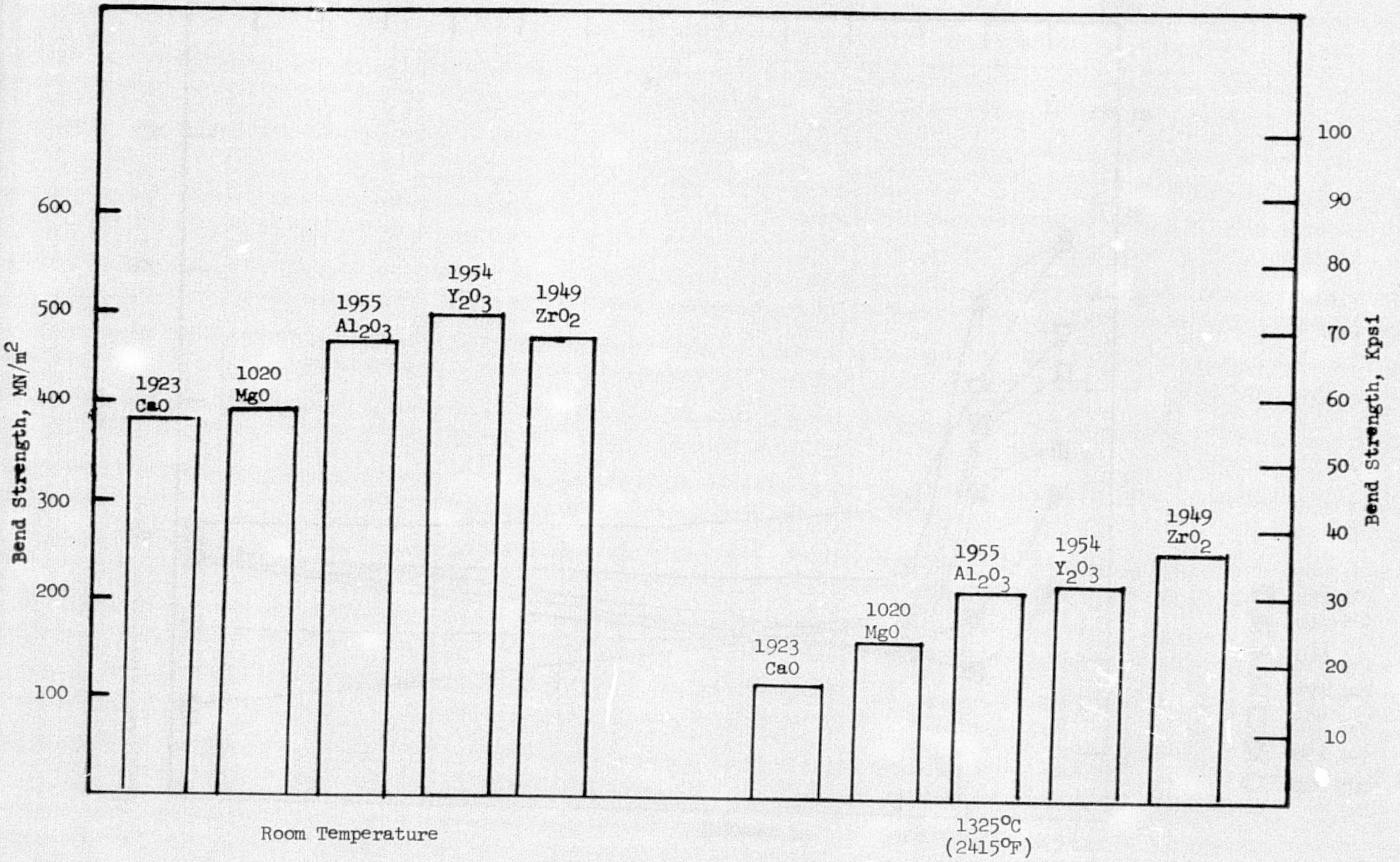

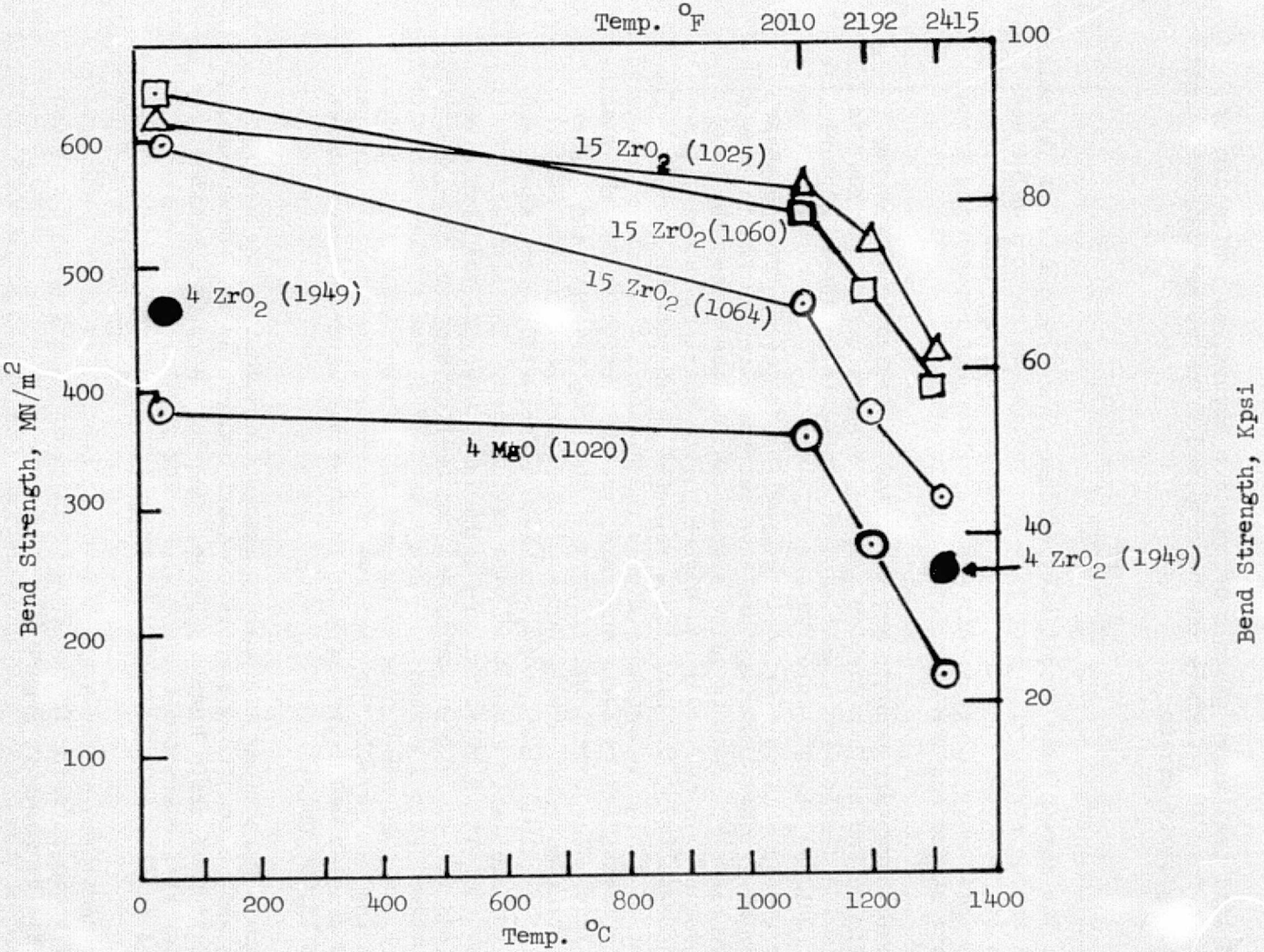

Figure 25. Bend Strength vs. Temperature Plots for Various Silicon Nitride Compositions Containing ZrO_2 Additive, Compared to CPG with 4 w/o MgO.

where σ = transverse rupture strength in psi,

P = load in pounds required to fracture,

b = specimen width in inches, and

h = specimen thickness in inches.

For a dead load test where plastic deformation occurs, an indication of the deviation from this formula can be obtained from the approximate equation for the steady-state stress:

$$\sigma = \frac{Pa}{bh^2} \quad (2 + m)$$

where m is the strain rate sensitivity exponent. For metals, m is typically 0.2 to 0.3 so the stress will drop from its initial value to a value near that given by the above equation. For ceramics, m is typically between 0.5 and 1.0 so that there is often only a small difference between the actual steady-state stress and the calculated elastic stress.

The stress rupture results are tabulated in Tables 11 and 12 for silicon nitride and silicon carbide samples, respectively. The results for silicon nitride demonstrate significant improvements in stress rupture life at 1100°C (2010°F), 1200°C (2192°F) and 1325°C (2415°F) for samples containing higher purity silicon nitride in comparison to the controlled phase grade material. Other investigators have reported similar findings on a comparative basis[10]. What is quite significant is the effect the ZrO_2 additive has on both the lower and higher purity starting material and follows the results of the bend tests reported in an earlier section. The development of a high temperature stable phase, i.e., a zirconium oxynitride, tentatively identified by X-ray analysis, probably accounts for the stability under load. The beneficial effects of the ZrO_2 additive and higher purity starting material are illustrated in Figure 26 where the 2415°F data for billets 1020, 1025, 1064, and 1966 are plotted; short time bend test data for similarly sized test bars is included. The similarities in data slopes indicate similar failure mechanisms; however, the strain was markedly less for the higher purity silicon nitride samples, e.g., < 0.5 percent compared to > 1 percent. A comparison of stress rupture behavior between billets 1020 AME-8 plus 4% MgO and 1122 forged AME-8 plus 4% MgO is interesting and reveals the positive effects developed texture may have. The forged samples had a life of 5 to 10 times the unforged materials at 2415°F and 15,000 psi.

The grain morphology and texture appear equivalent in the microstructures and no conclusions could be drawn concerning the concentration or distribution of grain boundary phase. The test samples exhibited fracture surfaces characteristic of slow crack growth, but no marked differences in this behavior could be found.

Other additives at the 4 wt. % level to controlled phase grade powder were found to be inferior to the ZrO_2 additive in 1325°C (2415°F) stress rupture tests as shown in Figure 27.

Although there is no hard evidence to identify the operative creep mechanism, it is assumed that creep is controlled by grain boundary sliding and its accommodation, which likely involves diffusion through the boundary phase. A major contributing cause of this behavior would appear to lie

Table 11. Stress Rupture Results for Si_3N_4

Billet	Material	Temperature °C	Temperature (°F)	Stress MN/m²	Stress (Kpsi)	Time to Failure (hours)	Strain (%)
1954	AME-8 Controlled Phase Grade Si_3N_4 + 4 w/o Y_2O_3	1325	(2415)	103.1	(15)	.63	0.4
				68.8	(10)	30.5	
				137.6	(20)	0.1	
1949	AME-8 Si_3N_4 + 4 w/o ZrO_2			137.6	(20)	0.1	0.5
				104.5	(15.2)	56.6	
				68.8	(10)	3.0 - no break	
1851	Controlled Phase Grade Si_3N_4 + 1 w/o MgO	1316	(2400)	103.1	(15)	4.2	
				89.4	(13)	55.1	0.6
				68.1	(9.9)	219.4	1.2
				61.9	(9)	304.6	1.4
1705	Controlled Phase Grade Si_3N_4 + 4 w/o MgO			103.1	(15)	3.43	
1923	AME Supergrade Si_3N_4 + 4 w/o CaO	1325	(2415)	103.1	(15)	.029	
1955	AME-8 Si_3N_4 + 4 w/o Al_2O_3			103.1	(15)	.037	
1963	9-1 + 4 w/o MgO			103.1	(15)	46.5	0.1
1966	9-2 + 4 w/o MgO			103.1	(15)	133.4 - no break	0.3
1966	9-2 + 4 w/o MgO			137.6	(20)	46.5	0.1
1049	9-4 + 4 w/o MgO			137.6	(20)	7.9	
1049	9-4 + 4 w/o MgO			103.1	(15)	30.7	
1061	9-4 + 1 w/o MgO			137.6	(20)	7.4	

Table 11 cont.

Billet	Material	Temperature °C	Temperature (°F)	Stress MN/m²	Stress (Kpsi)	Time to Failure (hours)	Strain (%)
1061	9-4 + 1 w/o MgO	1325	(2415)	103.1	(15)	163 - did not fail	0.3
1055	9-5 + 4 w/o MgO			137.6	(20)	1.4	
1070	9-6 + 4 w/o MgO			137.6	(20)	114 - did not fail	0.3
1070	9-6 + 4 w/o MgO			171.9	(25)	114 - did not fail	0.4
1070	9-6 + 4 w/o MgO			206.3	(30)	13.4	
1071	9-6 + 1 w/o MgO			103.1	(15)	63.4	0.2
1071	9-6 + 1 w/o MgO			137.6	(20)	2.3	
1020	AME-8 + 4 w/o MgO			103.1	(15)	1.8	
1020	AME-8 + 4 w/o MgO			68.8	(10)	4.1	
1122	Forged AME-8 + 4 w/o MgO			103.1	(15)	19.6	
1122	Forged AME-8 + 4 w/o MgO			103.1	(15)	11.7	
1123	Forged 9-1 + 4 w/o MgO			103.1	(15)	87.9	0.5
1025	9-2 + 15 w/o ZrO_2			137.6	(20)	110 - did not fail	0.1
1025	9-2 + 15 w/o ZrO_2			171.9	(25)	115 - did not fail	0.2
1025	9-2 + 15 w/o ZrO_2			206.3	(30)	161 - did not fail	0.3
1025	9-2 + 15 w/o ZrO_2			240.6	(35)	0.2	

Table 11 cont.

Billet	Material	Temperature °C	Temperature (°F)	Stress MN/m²	Stress (Kpsi)	Time to Failure (hours)	Strain (%)
1064	AME-8 Si_3N_4 + 15 w/o ZrO_2	1325	(2415)	103.1	(15)	62.1	0.3
1064	AME-8 Si_3N_4 + 15 w/o ZrO_2			68.8	(10)	115 - no break	0.4
1060	9-4 + 15 w/o ZrO_2			171.9	(25)	110 - no break	0.2
1060	9-4 + 15 w/o ZrO_2			206.3	(30)	75.2	0.1
1025	9-2 + 15 w/o ZrO_2	1200	(2192)	275.2	(40)	140 - no break	0.4
1025	9-2 + 15 w/o ZrO_2			309.4	(45)	1.6	
1020	AME-8 + 4 w/o MgO			103.1	(15)	161.9 - no break	0.9
1020	AME-8 + 4 w/o MgO			137.6	(20)	6.8	
1064	AME-8 + 15 w/o ZrO_2			137.6	(20)	48.1	0.5
1064	AME-8 + 15 w/o ZrO_2			103.1	(15)	121 - no break	
1049	9-4 + 4 w/o MgO			137.6	(20)	120.2 - no break	
1049	9-4 + 4 w/o MgO			171.9	(25)	53.1	
1966	9-2 + 4 w/o MgO			171.9	(25)	130 - no break	
1966	9-2 + 4 w/o MgO			206.3	(30)	38.2	
1025	9-2 + 15 w/o ZrO_2	1100	(2010)	309.4	(45)	122 - no break	0.4
1025	9-2 + 15 w/o ZrO_2			343.8	(50)	62.1	

Table 11 concl'd

Billet	Material	Temperature °C	Temperature (°F)	Stress MN/m²	Stress (Kpsi)	Time to Failure (hours)	Strain (%)
1020	AME-8 + 4 w/o MgO	1100	(2010)	137.6	(20)	116.5 - no break	1.1
1020	AME-8 + 4 w/o MgO	↓	↓	206.3	(30)	19.2	
1966	9-2 + 4 w/o MgO			240.6	(35)	110 - no break	
1966	9-2 + 4 w/o MgO			309.4	45	42	

Table 12. Stress Rupture Results for SiC

Billet	Material	Additive	Temperature °C (°F)	Stress MN/m² (Kpsi)	Time to Failure (hours)
2080	PPG SiC	1½ w/o C 1½ w/o Al_2O_3	1325 (2415)	103.1 (15)	137.2 - no break
				137.6 (20)	161.6 - no break
				206.3 (30)	138.8 - no break
				240.6 (35)	114.6 - no break
				309.4 (45)	140.3 - no break
				343.8 (50)	112.8 - no break
				412.5 (60)	Immediate failure
				378.1 (55)	Immediate failure
2080	PPG SiC	1½ w/o C 1½ w/o Al_2O_3	1200 (2192)	378.1 (55)	0.01
2080	PPG SiC	1½ w/o C 1½ w/o Al_2O_3		343.8 (50)	110 - no break
2080	PPG SiC	1½ w/o C 1½ w/o Al_2O_3	1100 (2010)	378.1 (55)	102 - no break
2080	PPG SiC	1½ w/o C 1½ w/o Al_2O_3		412.5 (60)	0.02

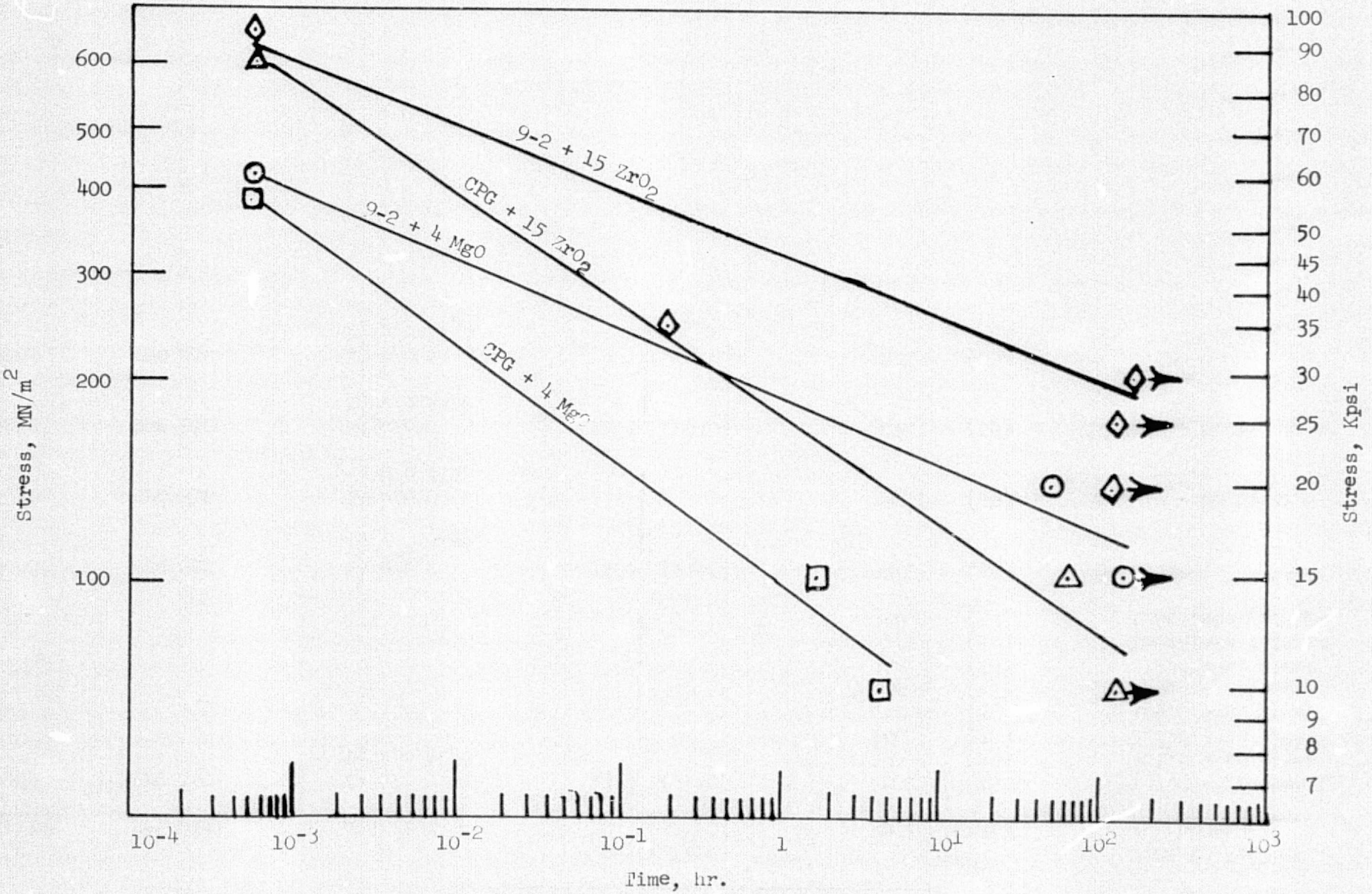

Figure 26. Bend Stress Rupture Plot for Silicon Nitride Compositions at 1385°C (2415°F).

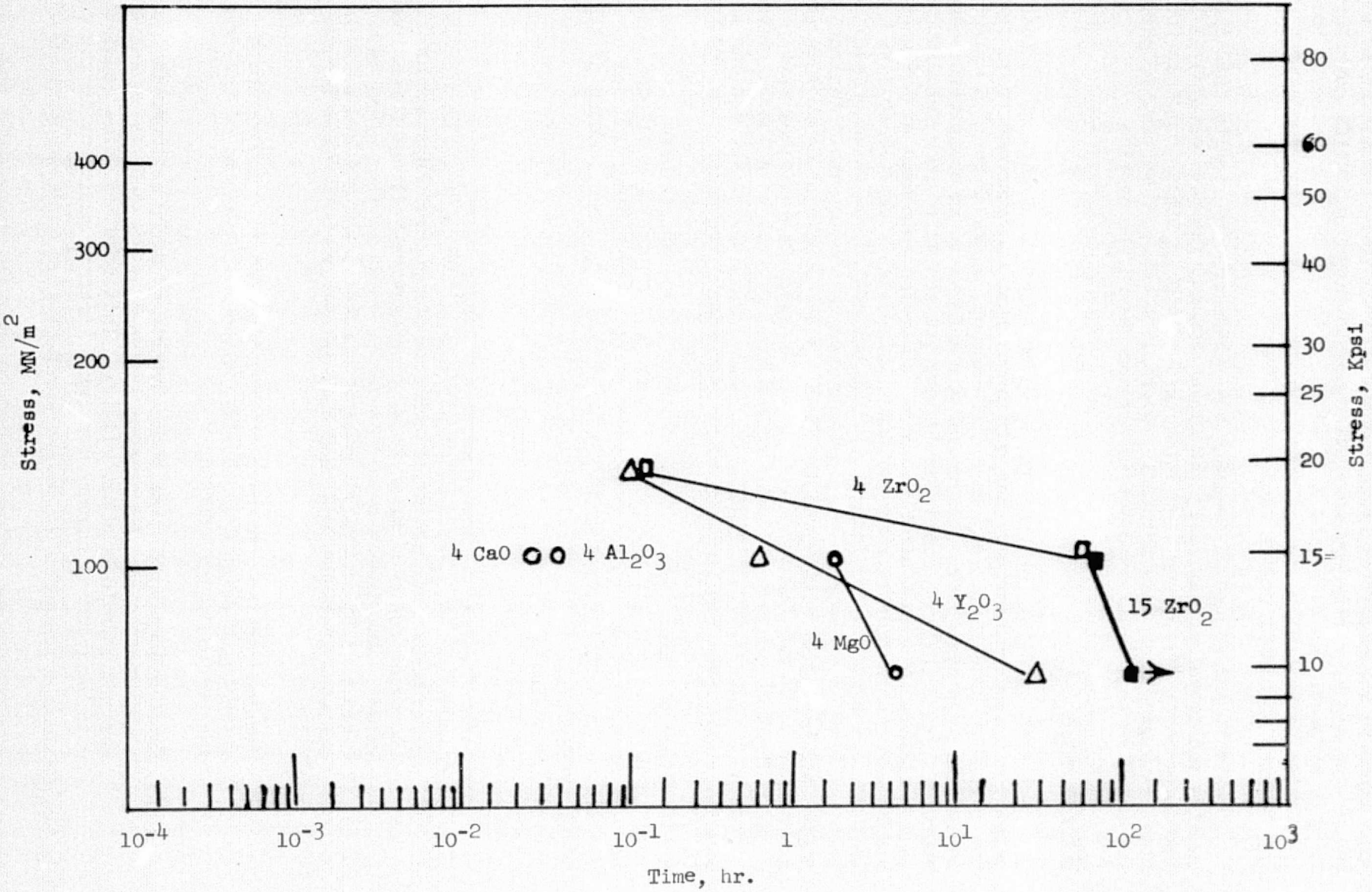

Figure 27. Bend Stress Rupture Plot for CP Grade Silicon Nitride with Various Additives at 1325°C (2415°F).

with improved accommodation brought about by boundaries containing silicate phase--the higher purity raw material demonstrating significant superiority in this respect. However, the ZrO_2 additive to AME-8 grade improves the properties dramatically, to the point where they are about "equivalent" to the samples of higher purity Si_3N_4 with standard MgO additive.

Table 12 and Figure 28 document the stress rupture results for silicon carbide and reveal dramatically the stress sensitivity (low slopes) by the immediate onset of failure when it occurs. There is little evidence for slow crack growth in this material. Overall, the stress rupture properties are superior to the maxima observed for the best Si_3N_4 samples.

Thermal Shock

A thermal cycling test was performed on selected samples of silicon carbide and sioicon nitride. The particular test has been described in the report of an earlier program[6]. The samples, wedge-shaped, 5 cm (2") in length, were heated by a mixture of air and gas to an equioibrium temperature of 1325°C (2415°F), held for an hour and cooled to room temperature in 2-3 minutes by a cold air blast directed at the thin edge of the wedge-shaped samples. After every 20 cycles, the specimens were removed from the test rig and examined for integrity. A total of 100 cycles comprised the test and both Si_3N_4 samples employed survived the test. These included a sample of 9-2 sublot with 4 w/o MgO (1966) and a sample of controlled phase grade with 4 w/o MgO (1020). Two SiC samples were tested along with the Si_3N_4. These included a PPG SiC (billet 2080) as well as a coarse grained Carborundum grade material similar to samples prepared in the earlier program[6]. The latter survived the cycle; however, the sample containing the PPG SiC failed between the 23rd and 38th cycle. These results are consistent with the findings of prior years efforts wherein Si_3N_4 samples have never failed in this particular test; however, a number of SiC samples have been observed to fail in mid-cycle. The higher coefficient of expansion, modulus of elasticity, and rapid crack growth extensions for SiC are factors of significance here.

CONCLUSIONS

The major findings of this program are listed below.

1. Silicon nitride impact strengths showed general improvement over previous results in terms of consistency if not in maximum values. The target of 0.7 joules (6 in-lbs.) (for 0.635 cm x 0.635 cm (.25" x .25") cross-section bars) was reached only in isolated instances and then only in samples taken from forged billets.

2. Silicon carbide continued to show significantly lower impact strengths than silicon nitride, although the extent of the testing performed was limited.

3. The elevated short time bend strength of Si_3N_4 is improved significantly by improvements in impurity content, which apparently restricts grain boundary sliding. This result is also consistent with bend stress rupture testing. Zirconia additives in the form

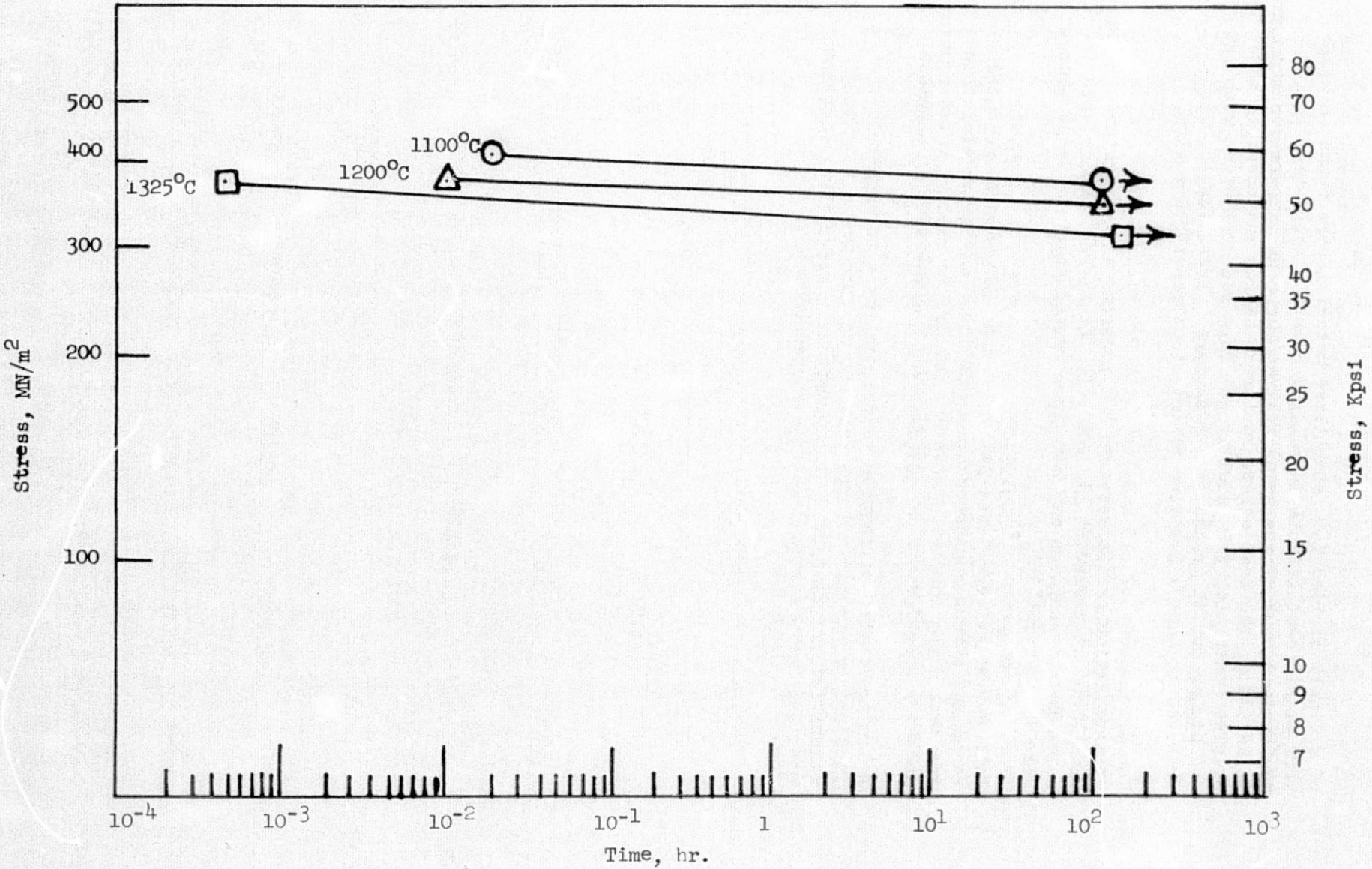

Figure 28. Bend Stress Rupture Plot for Silicon Carbide (2080).

of a finely divided Y_2O_3 stabilized material were found to have very significant effects in raising both the short term low temperature bend strengths as well as the high temperature strengths. In addition, the best stress rupture behavior was observed with samples containing ZrO_2 additions. This was consistent with low and higher purity grades of AME powders. Press forging was observed to have a positive effect on stress rupture life.

4. The development of SiC samples, with PPG starting powders, with isotropic fine grains required hot pressing at temperatures below 2000°C and at pressures of 8000 psi. At higher temperatures the rapid $\beta \rightarrow \alpha$ transition may have been responsible for large plate-like grain formation.

5. Bend stress rupture tests performed with SiC samples revealed excellent stress rupture characteristics - maxima greater than the best Si_3N_4 samples. However, failure is rapidly catastrophic and slow crack growth is not observed for the samples prepared.

6. A limited number of samples tested continues to reinforce the findings of earlier efforts that SiC is more prone to thermal stress failure than Si_3N_4 in a particular air cycling environment and for a particular wedge-shaped geometry.

REFERENCES

1. F.F. Lange and G.R. Terwilliger, "Fabrication and Properties of Silicon Compounds", Final Report, Contract N00019-17-C-0107.

2. W.H. Rhodes and R.M. Cannon, Jr., "High Temperature Compounds for Turbine Vanes", NASA CR 134531, January 1974.

3. G. Gazza, "Effect of Y_2O_3 Additions on Properties of Silicon Nitride," Annual Meeting of American Ceramic Society (May 1974).

4. P. Grieveson, K.H. Jack, and S. Wild, "The Crystal Chemistry of Ceramic Phases in the Silicon-Nitrogen-Oxygen and Related Systems", Progress Report 5, Ministry of Defense Contract N/C P.61/9411/67/4B/MP.387 (June 1970).

5. R.M. Cannon, Jr. and R.J. Hill, "High Temperature Compounds for Turbine Vanes," NASA CR 72794 (1970).

6. W.H. Rhodes and R.M. Cannon, Jr., "High Temperature Compounds for Turbine Vanes," NASA CR-120966 (1972).

7. W.H. Rhodes and R.M. Cannon, Jr., "Microstructure Studies of Polycrystalline Refractory Compounds", Contract N00019-73-C-0376.

8. F.F. Lange, "Theory on Dispersion Toughening of Brittle Ceramics", Contract N0014-68-C-0323.

9. W. McDonough and R. Rice, "Effect of ZrO_2 Addition on Properties of Silicon Nitride," Annual Meeting of Am. Ceram. Soc., Washington, D.C. (May 1975).

10. F.F. Lange and J.L. Iskoe, "High Temperature Strength Behavior of Hot Pressed Si_3N_4 and SiC: Effect of Impurities", Proc. Army Materials Tech. Conf. on Ceramics for High Performance Applications (in press).